Bioactive Materials 19 (2023) 24–37

Contents lists available at ScienceDirect

Bioactive Materials

journal homepage: www.keaipublishing.com/en/journals/bioactive-materials

Sequential gastrodin release PU/n-HA composite scaffolds reprogram macrophages for improved osteogenesis and angiogenesis

Limei Li [a,1], Qing Li [a,1], Li Gui [b], Yi Deng [c], Lu Wang [a], Jianlin Jiao [a], Yingrui Hu [a], Xiaoqian Lan [d], Jianhong Hou [e,***], Yao Li [f,**], Di Lu [a,*]

[a] Yunnan Key Laboratory of Stem Cell and Regenerative Medicine, Science and Technology Achievement Incubation Center, Kunming Medical University, Kunming, 650500, China
[b] Department of Endocrinology, The Third People's Hospital of Yunnan Province, Kunming, 650011, China
[c] School of Chemical Engineering, State Key Laboratory of Polymer Materials Engineering, Sichuan University, Chengdu, 610065, China
[d] Department of Neurology, The First Affiliated Hospital, Kunming Medical University, Kunming, 650000, China
[e] Department of Orthopaedics, The Third People's Hospital of Yunnan Province, Kunming, 650011, China
[f] Department of Stomatology, The First People's Hospital of Yunnan Province, Kunming, 650032, China

ARTICLE INFO

Keywords:
Gastrodin-delivery
Immune/inflammatory response
Osteogenesis
Angiogenesis
Tissue repair

ABSTRACT

Wound healing is a highly orchestrated process involving a variety of cells, including immune cells. Developing immunomodulatory biomaterials for regenerative engineering applications, such as bone regeneration, is an appealing strategy. Herein, inspired by the immunomodulatory effects of gastrodin (a bioactive component in traditional Chinese herbal medicine), a series of new immunomodulatory gastrodin-comprising biodegradable polyurethane (gastrodin-PU) and nano-hydroxyapatite (n-HA) (gastrodin-PU/n-HA) composites were developed. RAW 264.7 macrophages, rat bone marrow mesenchymal stem cells (rBMSCs), and human umbilical vein endothelial cells (HUVECs) were cultured with gastrodin-PU/n-HA containing different concentrations of gastrodin (0.5%, 1%, and 2%) to decipher their immunomodulatory effects on osteogenesis and angiogenesis *in vitro*. Results demonstrated that, compared with PU/n-HA, gastrodin-PU/n-HA induced macrophage polarization toward the M2 phenotype, as evidenced by the higher expression level of pro-regenerative cytokines (CD206, Arg-1) and the lower expression of pro-inflammatory cytokines (iNOS). The expression levels of osteogenesis-related factors (BMP-2 and ALP) in the rBMSCs and angiogenesis-related factors (VEGF and BFGF) in the HUVECs were significantly up-regulated in gastrodin-PU/n-HA/macrophage-conditioned medium. The immunomodulatory effects of gastrodin-PU/n-HA to reprogram macrophages from a pro-inflammatory (M1) phenotype to an anti-inflammatory and pro-healing (M2) phenotype were validated in a rat subcutaneous implantation model. And the 2% gastrodin-PU/n-HA significantly decreased fibrous capsule formation and enhanced angiogenesis. Additionally, 2% gastrodin-PU/n-HA scaffolds implanted in the rat femoral condyle defect model showed accelerated osteogenesis and angiogenesis. Thus, the novel gastrodin-PU/n-HA scaffold may represent a new and promising immunomodulatory biomaterial for bone repair and regeneration.

1. Introduction

The treatment of large bone defects is a major medical problem worldwide. Biomaterial implantation is deemed an important option to promote bone reparation, but its efficiency remains a challenging issue [1–4]. Bone healing is a well-orchestrated process involving interactions among different complex biological events, including early inflammatory immune regulation, angiogenesis, osteogenic differentiation, and osteogenesis [5,6]. Various biomaterials have been investigated, with emphasis on the development of favorable bone substitutes with desired

Peer review under responsibility of KeAi Communications Co., Ltd.
* Corresponding author.
** Corresponding author.
*** Corresponding author.
E-mail addresses: hjhjyy@126.com (J. Hou), 2771908707@qq.com (Y. Li), ludi20040609@126.com (D. Lu).
[1] These authors contribute equally to this work.

https://doi.org/10.1016/j.bioactmat.2022.03.037
Received 3 December 2021; Received in revised form 4 March 2022; Accepted 23 March 2022

physiochemical [7,8], mechanical [9,10], and osteogenic properties [11,12] related to bone formation. However, the often-ignored regulatory role of the immune system in the biomaterial-mediated bone microenvironment can lead to undesirable bone repair effects [13]. After implantation *in vivo*, biomaterials interact with immune cells and can trigger an inflammatory response, with the cell types involved and duration of the response markedly affecting therapeutic indices, from fibrosis formation to regeneration (osteogenesis and angiogenesis) [14]. An unrestrained inflammatory response can disrupt bone homeostasis, resulting in delayed wound healing and bone tissue regeneration. In contrast, a beneficial anti-inflammatory immune microenvironment modulated by biomaterials could ensure better bone cell differentiation, improved blood vessel formation, and successful long-term implantation [15,16].

Macrophages, major immune cells that form the first line of defense in the immune system, play a central role in orchestrating immunoinflammatory responses and tissue repair by releasing cytokines, growth factors, and chemokines to determine the fate of biomaterials [17,18]. Indeed, macrophages have been widely targeted to investigate the osteoimmunomodulatory properties of biomaterials. Chang et al. reported that depletion of macrophages *in vivo* using the macrophage by Fas-L-induced apoptosis (MAFIA) mouse caused complete loss of osteoblast bone-forming, expressed lower mRNA of ALP and COL1 [19]. Deficiency in macrophages also significantly inhibits the deposition of woven bone and mineralization of new bone in mouse models with tibia defects [20]. In response to different microenvironments, macrophages polarize towards different phenotypes, including pro-inflammatory (M1) and pro-healing (M2) polarization, which exert different effects on tissue repair [21]. In the inflammation phase, macrophages tend to polarize towards the M1 phenotype, which promotes the secretion of pro-inflammatory cytokines such as tumor necrosis factor-alpha (TNF-α), interleukin-1 beta (IL-1β), and inducible nitric oxide synthase (iNOS), which can exacerbate harmful inflammatory responses [22,23]. In the repair phase, macrophages in the M2 phenotype generally express high levels of interleukin-10 (IL-10), arginase-1 (Arg-1), bone morphogenetic protein 2 (BMP-2), and vascular endothelial growth factor (VEGF), which suppress inflammation, recruit osteoprogenitor cells, and activate angiogenesis, tissue remodeling, and bone regeneration [24,25]. Aberrant immunomodulation (suppression or enhancement) may delay bone regeneration by blocking the transformation of macrophages from the M1 to M2 phenotype [14,26]. Therefore, a combined immunomodulatory tool capable of effectively controlling the density of activated M2 macrophages at the early stage of bone injury could significantly influence bone healing events and the *in vivo* fate of bone repair biomaterials [27–29].

M2 macrophages contribute to satisfactory bone repair and construction. Of note, they can be modulated by tailoring the properties of biomaterials to create a favorable immune microenvironment [30,31]. Understanding macrophage-biomaterial interactions through positive feedback with the immune system is important for designing synthetic bone grafts with improved features to foster bone formation [32]. An innovative strategy has been developed to optimize immunomodulatory biomaterials that harmonize M1-M2 polarization [33,34]. To this end, the tailorable cues of biomaterials regarding surface topography, hydrophilicity, porosity, and materials dynamics and mechanics [35–37] can be considered for modulating the macrophage immune response. The main bioactive constituents of the traditional Chinese herbal medicines (e.g., Icariin [38], curcumin [39]) have also been applied to immunomodulation because of their anti-inflammatory properties and bone healing-enhancing effects. However, due to their complex chemical structure, the constituents are rarely used as a chemical synthesis component of biomaterials. The common application strategies are intragastric administration, physical mixing with materials and microsphere sustained release, which reduce immunomodulatory performance.

Gastrodin, a primary bioactive constituent of traditional Chinese herbal medicine with potential immunomodulatory capacities, is used as an inherent drug for therapeutic development [40–42]. Gastrodin can protect stem cells against oxidative stress and dysfunction and improve osteogenic markers [43], and act as an osteodifferentiation molecule to promote mineralization dose dependently [44]. When used for sustained delivery, the pharmacokinetics, biodistribution, and mechanisms of gastrodin may modulate the immune system. Compared with other traditional Chinese medicines, gastrodin has a relatively simple chemical structure and polyhydroxyl functional group, which can be chemically polymerize. Of note, polyurethane (PU) has binding sites at chain segments and been widely used to deliver drugs to augment healing outcomes [45,46], holding great promise as a superior functional material in tissue engineering [47–50]. Thus, gastrodin bound to PU not only enhances mechanical properties as a cross-linker, but also increases hydrophilicity to facilitate cell adhesion [51]. These attractive features encourage us to synthesize anti-inflammatory gastrondin/PU for vascular tissue engineering in previous report [52]. However, there has been a dearth of research on gastrodin into bone biomimetic degradable materials for osteoimmunomodulation. PU/nano-hydroxyapatite (PU/n-HA) composites, which are widely used biomaterials in bone regeneration, possess excellent osteoconductive and osteoinductive properties and a similar chemical composition and hierarchical structure as natural bone [53–55]. Based on these advantageous features, we wondered whether PU/n-HA and gastrodin in combination could optimize their functions.

To achieve this, we developed a novel system combining bioactive gastrodin and bionic PU/n-HA scaffolds for the treatment of bone defects. The scaffold provided on-demand drug release, depending on the progressive degradation of PU in response to the components. Moreover, the sequential gastrodin-delivery PU/n-HA scaffolds reprogrammed the M2 macrophage domain to trigger osteogenic effects of the activated osteoimmune environment on rat bone marrow mesenchymal stem cells (rBMSCs) as well as angiogenic effects on human umbilical vein endothelial cells (HUVECs). The adaptive immune/inflammatory response also initiated the production of pro-healing cytokines against pro-inflammatory cytokines and activated angiogenesis in subcutaneous implantation. Finally, the optimized gastrodin-PU/n-HA scaffolds efficiently enhanced vascular bone tissue regeneration using a femoral condyle defect model in rats. The present study sheds light on the significance of immunomodulatory gastrodin-PU/n-HA with multi-effective bone regeneration capacity in orthopedic fields.

2. Materials and methods

2.1. Chemicals and reagents

Poly(Ɛ-caprolactone)2000 (PCL2000), isophorone diisocyanate (IPDI), and lysine ethyl ester dihydrochloride (Lys·OEt–2HCl) were purchased from Aladdin Co., Ltd. (China). The n-HA powder was prepared using a previously reported hydrothermal method [55], then sifted through sieves (300 mesh diameter). Gastrodin (purity >99.0%) was purchased from Kunming Pharmaceutical Co., Ltd. (China). The other AR-grade chemicals were purchased from Tianjin Fengchuan Chemical Reagent Technology (China). All chemicals were used as received without further purification unless otherwise stated.

2.2. Preparation of porous composite scaffolds

Porous composite scaffolds were successfully constructed using the *in situ* foaming method [55]. First, 30.00 g of PCL2000 and 10.50 g of n-HA (20 wt%) particles were mixed in a 250-ml three-necked flask under a nitrogen atmosphere and heated at 70 °C, after which 7.80 g of IPDI was added with stirring for 4 h to obtain the prepolymer. Successively, 3.70 g of Lys·OEt–2HCl was applied as a chain extender to extend the prepolymer. After stirring for 2 h, different concentrations of gastrodin were added into the prepolymer to form four different scaffolds.

Finally, 0.2 ml of deionized water was added and stirred for 30 min. The resultant mixture was cured at 90 °C accompanied by simultaneous foaming. According to the theoretical weight ratio of gastrodin in the polymer chain (set as 0%, 0.5%, 1%, and 2%), the samples were named as PU/n-HA, 0.5%, 1%, and 2% gastrodin-PU/n-HA, respectively.

2.3. Characterization of scaffolds

2.3.1. Fourier transform infrared spectroscopy (FTIR) analysis

The functional structure of scaffolds was investigated by FTIR using a spectrometer (ThermoFisher, Nicoletis10, USA). The FTIR spectra were collected in the range of 4000–600 cm^{-1}.

2.3.2. X-ray diffraction (XRD) analysis

The XRD patterns of pure n-HA and scaffolds incubated in 0.5 M NaOH solution for 0 and 12 weeks were determined by XRD (KAlpha+, ThermoFisher Scientific, USA) at 40 kV and 20 mA in a 2θ range of 5–60° with a step of 0.03°.

2.3.3. Mechanical test

The compressive strength and modulus of specimens (10 × 10 × 20 mm^3) were measured using a universal testing machine (AUTOGRAPH AG-IC 20/50 KN, Japan). The cross-head speed was set to 5 mm/min, and the load was applied until the specimen was compressed to 40% of its original length. Five specimens in each group were subjected to this test.

2.3.4. In vitro degradation studies

The scaffolds (~0.21 g) were subjected to a degradation test in 3 ml of 0.5 M NaOH solution at 37 °C, which accelerated degradation. The experiment was performed in quintuplicate. The initial weight was noted as W_0. The specimens were removed from the NaOH solution at 1, 2, 4, 6, 8, 10, and 12 weeks, then washed with distilled water, dried, and weighed. The final weight was noted as W_1. Mass loss was calculated according to the following equation:

$$\text{Mass loss} = [(W_0 - W_1) / W_0] \times 100\%$$

At the time point of degradation, the accumulated suspension liquor was measured to evaluate gastrodin release by high-performance liquid chromatography (HPLC, Shimadzu, Kyoto, Japan) at a wavelength of 220 nm. Detailed procedures are provided in the Supplementary Information (SI).

2.4. Cell viability study in vitro

After sterilization by γ-ray irradiation with 15 kGy, scaffold discs (Φ 13 mm × 2 mm) were incubated with rBMSCs (2×10^4 cells/well) in 24-well plates using Minimum Essential Medium Alpha (α-MEM, Corning, USA) supplemented with 10% fetal bovine serum (FBS, Gibco, USA), 1% penicillin-streptomycin (HyClone, USA) for 4 and 7 days (n = 5). The cell culture medium was replaced every 3 days. At each time point, the culture medium was removed and washed twice with phosphate-buffered saline (PBS). A Live/Dead Viability/Cytotoxicity Assay Kit (ThermoFisher Scientific, USA) was used for fluorescence staining of live (green) and dead (red) cells. The scaffolds with adherent cells were rinsed with PBS three times, stained by live/dead solution, and incubated at 37 °C for 0.5 h to monitor rBMSC viability. Images were captured using an inverted fluorescence microscope (IX73, Olympus, Japan). In addition, cells washed with PBS were stained with Mito-Tracker® Red CMXRos (Solarbio, China, No.: M9940) for cytoplasmic mitochondria and incubated at 37 °C for 0.5 h. After fixation with 4% paraformaldehyde solution, the cells were stained with phalloidin (Solarbio, China, No.: CA1640) for actin and DAPI (Abcam, USA, No: ab104139) for nuclei and then imaged using an optical microscope (BX53, Olympus, Japan). Cell proliferation was further evaluated using a Cell Counting Kit-8 (CCK-8) assay (Dojindo Molecular Technologies, Japan).

To explore the effects of scaffolds on osteogenic differentiation, rBMSCs (2×10^4 cells/well) were seeded onto scaffolds in 24-well plates and incubated with α-MEM. After culturing for 14 days, the cells were extracted by TRIzol reagent (ThermoFisher Scientific, USA) and analyzed by RT-qPCR. The expression levels of runt-related transcription factor 2 (RUNX2), alkaline phosphatase (ALP), and collagen type 1 (COL1) were measured.

2.5. Immune/inflammatory response in vitro

2.5.1. Immunomodulatory effects of scaffolds on RAW 264.7 cells

RAW 264.7 cells (leukemia cells in mouse macrophage cell line) (5×10^4 cells/well) were seeded onto scaffolds in 12-well plates with Dulbecco's Modified Eagle's Medium (DMEM, Corning, USA) supplemented with 10% FBS and 1% penicillin-streptomycin. After 3 days of incubation, the medium was collected and centrifuged to obtain the supernatant as the conditioned medium for subsequent experiments.

Cell proliferation was evaluated using the CCK-8 assay. Relative gene expression levels of iNOS, Arg-1, and cluster of differentiation 206 (CD206) were measured by RT-qPCR. Relative protein expression levels of Arg-1, CD206, iNOS, and TNF-α were measured by western blotting. For immunofluorescence analysis, cells were fixed in 4% paraformaldehyde solution for 30 min, permeabilized in 0.1% Triton X-100 for 30 min, and blocked in 10% goat serum for 6 h. The cells were incubated with primary antibodies against iNOS and Arg-1 at 4 °C overnight, respectively, then incubated with secondary antibodies for 2 h in the dark at room temperature. Cell nuclei were stained with DAPI and mounted. Protein expression in cells was detected with an optical microscope and optical density was calculated using Image Pro Plus v6.0 and GraphPad Prism v8.0.

2.5.2. Osteogenic differentiation of rBMSCs under macrophage microenvironment modulation

A special culture medium for rBMSCs was prepared by 2-fold dilution of the conditioned medium (see Section 2.5.1.) with fresh α-MEM. The rBMSCs (1×10^6 cells/well) were seeded in 6-well plates in the α-MEM for cell migration assay. After 12 h of incubation, a scratch was made using a sterile 200-μl pipette tip, and cell debris was washed with PBS. The special culture medium without FBS was then added to the wells. Cell migration propensity was imaged after 0 and 24 h. The wound areas were measured by Image Pro Plus v6.0. Furthermore, rBMSCs (1×10^5 cells/well) were seeded in 12-well plates in α-MEM to evaluate osteoimmune regulation. After 12 h of incubation, the original medium was removed and substituted with the special culture medium. After 3 days of culture, the rBMSCs were harvested and total RNA was extracted for analysis of osteogenic genes BMP-2 and ALP by RT-qPCR. Protein expression of BMP-2 was further evaluated by western blotting and immunofluorescence.

2.5.3. Angiogenesis analysis of HUVECs under macrophage microenvironment modulation

The special culture medium for HUVECs was prepared by mixing DMEM and collected conditioned medium (see Section 2.5.1.) at a ratio of 2:1. The HUVECs (1×10^6 cells/well) were seeded in 6-well plates in DMEM and subjected to cell migration assay. Furthermore, the cells (1×10^5 cells/well) were seeded in 12-well plates in DMEM to determine the effects of the macrophage microenvironment on HUVECs. After culturing for 12 h, the original medium was removed and replaced by the special culture medium for a further 3 days of incubation. Finally, the related angiogenic genes and proteins of VEGF and basic fibroblast growth factor (BFGF) were evaluated by RT-qPCR, western blotting, and immunofluorescence.

2.6. Immunomodulatory effect and angiogenesis of subcutaneously embedded scaffolds

24 Sprague-Dawley (SD) rats (males, 200–220 g) were used for subcutaneous implantation of scaffolds. All animal experimental protocols followed the guidelines and regulations of the Institutional Animal Care and Use Committee of Kunming Medical University (China). The rats were randomly divided into four groups (six rats/group): PU/n-HA, 0.5%, 1%, and 2% gastrodin-PU/n-HA. Each sterilized disc specimen (Φ 13 mm × 2 mm) was symmetrically transplanted into the dorsal subcutaneous pocket of each rat. All rats were then sacrificed at 3 and 14 days after implantation. Collected blood serum was assayed to measure the content of IL-1β using an IL-1β ELISA kit (Nanjing Jiancheng, China) according to the manufacturer's instructions. Vascular connections *ex vivo* were tested, with further details reported in the SI. Samples with the surrounding tissues along with the heart, liver, spleen, kidney, and lung were collected and fixed with 4% paraformaldehyde solution for 7 days. The tissue samples were dehydrated in graded concentrations of ethanol. After this, they were cleared in xylene, embedded in paraffin wax, and cut into 5-μm thick sections. The sections were deparaffinized, rehydrated, and stained hematoxylin and eosin (H&E), Masson, CD31, Arg-1, and iNOS, followed by imaging using an optical microscope.

2.7. Repair assay in rat femoral condyle defect model

The experiments involved the use of 45 SD rats. Based on the *in vitro* results, rats were divided into three groups: PU/n-HA, 1%, and 2% gastrodin-PU/n-HA. After exposure of the lateral femoral condyle, a defect (Φ 3 mm × 3 mm in size) was created. A sterilized scaffold (Φ 3 mm × 3 mm) was inserted into the defect, with the musculature and skin incision then closed with absorbable sutures. At postoperative weeks 4, 8, and 12, the rats were euthanized, and the femurs with implantations were harvested and fixed in 4% paraformaldehyde solution for micro-computed tomography (micro-CT) and histological and immunological examination. Further details are reported in the SI.

2.8. Statistical analysis

Data were reported as means ± standard deviation (SD). One-way analysis of variance (ANOVA) was applied for statistical comparisons among more than two groups, and *t*-test was used for statistical comparisons between two groups. All statistical analyses were performed using GraphPad Prism v8.0. Statistical significance was accepted at $P < 0.05$.

3. Results

3.1. Physicochemical properties of scaffolds

As shown in Fig. 1A, the peaks at 2936 cm^{-1} and 2864 cm^{-1} belonged to symmetric and asymmetric vibrations of the $–CH_3$ and $–CH_2$ groups, respectively. The peaks at 1723 cm^{-1} and 1529 cm^{-1} were ascribed to C = O and –NH stretching of the urethane group (OCONH) of PU, respectively. The characteristic peak at 3372 cm^{-1} for gastrodin was

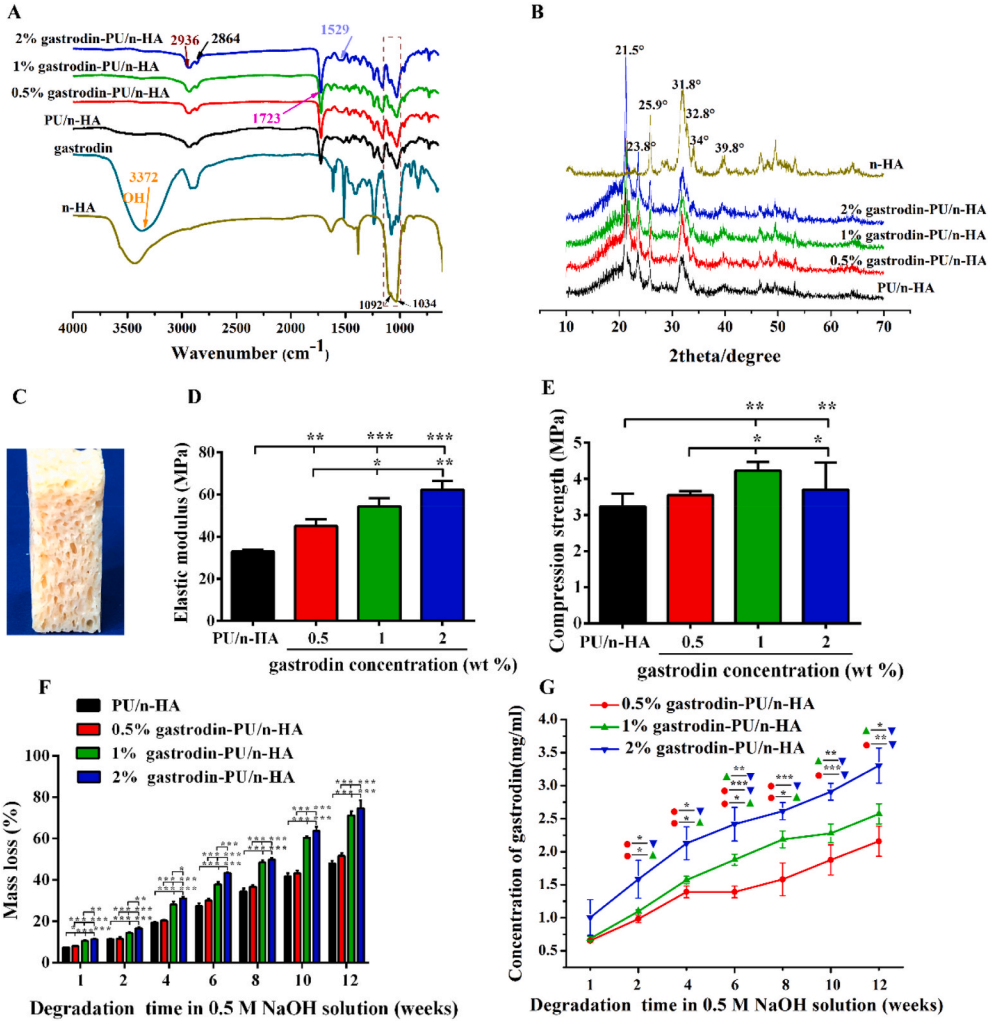

Fig. 1. (A) FTIR spectral characterization of n-HA, gastrodin, and gastrodin-PU/n-HA scaffolds. (B) XRD characterization of n-HA and gastrodin-PU/n-HA scaffolds. (C) Digital photo of scaffolds. (D, E) Effects of gastrodin concentration on mechanical properties: (D) Elastic modulus and (E) Compression strength. (F) *In vitro* degradation study of scaffolds in 0.5 M NaOH solution. (G) Gastrodin release profiles from scaffolds in 0.5 M NaOH solution. Error bars represent standard deviation from mean (n = 5). ***$p < 0.001$; **$p < 0.01$; *$p < 0.05$.

significantly reduced in PU, indicating its role in cross-link polymerization, as demonstrated in our previous report [51]. The broad peaks at 1092 cm^{-1} and 1034 cm^{-1} corresponded to the vibration of a phosphate group (PO_4), suggesting that n-HA was composited into the scaffolds. The band at 3431 cm^{-1} was due to –OH stretching mode in the crystal lattice of n-HA [56].

The XRD pattern also showed a typical n-HA crystalline structure in Fig. 1B. The peaks at 25.9° (002), 31.8° (211), 32.8° (300), 34.0° (202), and 39.8° (310) were characteristic of n-HA. Reduction in peak intensity of n-HA in the composites may result from its envelope within the PU matrix. Two distinct diffraction peaks were observed for all scaffolds at $2\theta = 21.5°$and 23.8° for the orthorhombic crystalline structure of PCL2000 (Fig. S3).

The scaffolds showed a porous morphology (Fig. 1C). Moreover, gastrodin had a positive effect on the mechanical properties of the PU scaffolds, as shown in Fig. 1D and E. The elastic moduli of 2% gastrodin-PU/n-HA (62.20 ± 4.28 MPa), 1% gastrodin-PU/n-HA (54.38 ± 3.89 MPa), and 0.5% gastrodin-PU/n-HA (45.05 ± 3.23 MPa) were significantly higher than that of the PU/n-HA group (32.90 ± 1.02 MPa) (Fig. 1D). Both 2% gastrodin-PU/n-HA (3.70 ± 0.75 MPa) and 1% gastrodin-PU/n-HA (4.79 ± 0.46 MPa) had relatively higher compression strengths than the other groups (0.5% gastrodin-PU/n-HA (3.54 ± 0.10 MPa) and PU/n-HA (3.24 ± 0.36 MPa)) (Fig. 1E).

The degradation profiles of the scaffolds in 0.5 M NaOH solution are shown in Fig. 1F. The degradation rate increased with the increase in gastrodin content in the PU. After 8 weeks, 2% and 1% gastrodin-PU/n-HA degraded by 49.78% and 48.43%, entering into a relatively rapid degradation period. In contrast, 0.5% gastrodin-PU/n-HA and PU/n-HA degraded only around 36.60% and 34.46%. At 12 weeks, the 2% gastrodin-PU/n-HA (74.60% ± 3.96%) and 1% gastrodin-PU/n-HA groups (71.17% ± 1.95%) had significantly higher degradation rates than that of the 0.5% gastrodin-PU/n-HA (51.60% ± 1.32%) and PU/n-HA groups (48.07% ± 1.15%) ($p < 0.001$) (Fig. 1F). The intensity of peaks in n-HA and PCL2000 also decreased after 12 weeks of degradation (Fig. S6). According to gastrodin release (Fig. 1G), the 2% gastrodin-PU/n-HA scaffold exhibited a sequential gastrodin release profile, showing an initial release level of 1.0 mg/ml in the first week and a total release level of 3.3 mg/ml after 12 weeks. Of note, gastrodin release from the 0.5% and 1% gastrodin-PU/n-HA scaffolds was significantly lower than that released from the 2% gastrodin-PU/n-HA scaffold after 12 weeks.

3.2. rBMSC activity and differentiation

To investigate the effects of gastrodin-delivery PU/n-HA on cellular behavior, rBMSCs were cultured on the scaffolds. Live/dead results

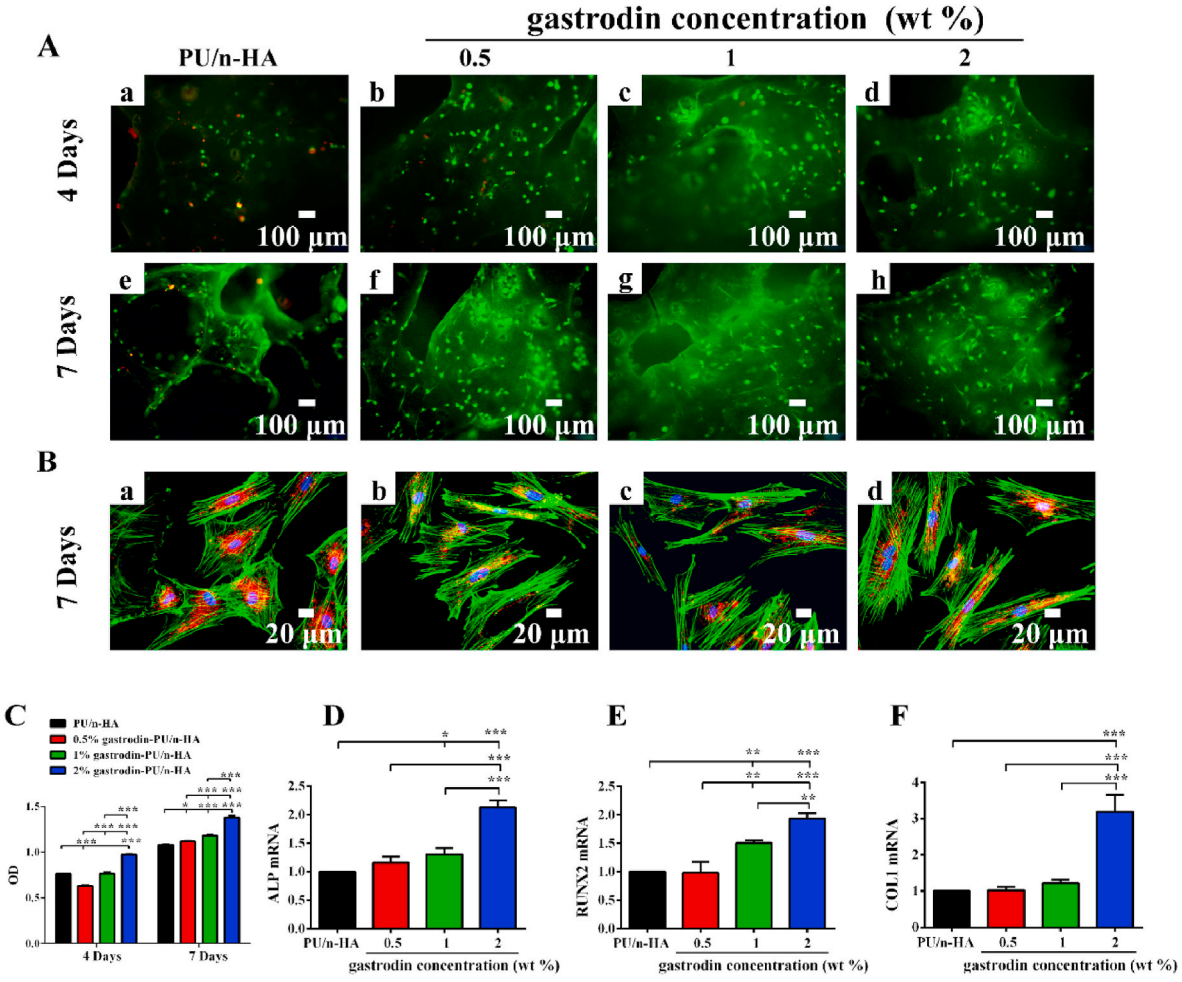

Fig. 2. *In vitro* viability and osteogenic differentiation of rBMSCs cultured on scaffolds. (A) Live/dead staining of rBMSCs on scaffolds after 4 and 7 days: (a, e) PU/n-HA, (b, f) 0.5% gastrodin-PU/n-HA, (c, g) 1% gastrodin-PU/n-HA, and (d, h) 2% gastrodin-PU/n-HA. Live cells are stained green, dead cells are stained red. (B) Images showing rBMSC morphology after 7 days of culture. F-actin is stained green, cytoplasmic mitochondria are stained red, and nuclei are stained blue. (C) CCK-8 assay for proliferation after 4 and 7 days. (D–F) Relative expression of osteogenic genes (ALP, RUNX2, COL1) in rBMSCs cultured on composite scaffolds for 14 days. Error bars represent standard deviation from mean (n = 5). ***$p < 0.001$; **$p < 0.01$; *$p < 0.05$. (For interpretation of the references to colour in this figure legend, the reader is referred to the Web version of this article.)

showed that cells adhered and grew on the surface of each scaffold on days 4 and 7 (Fig. 2A). Furthermore, cell proliferation increased with prolonged culture time. Dead rBMSCs (in red) were found on the PU/n-HA scaffold, and the number of cells was markedly lower than that found on the gastrodin-PU/n-HA scaffolds. Cell proliferation, as determined via the CCK-8 assay (Fig. 2C), further demonstrated that the number of rBMSCs increased with culture time and gastrodin concentration, thus showing good cytocompatibility. Most rBMSCs exhibited highly stretched morphology with many long extension processes (Fig. 2B). On the other hand, the gastrodin-PU/n-HA groups induced higher osteogenic differentiation compared to the PU/n-HA group, confirming the superior osteo-promotive effects of gastrodin-PU/n-HA over PU/n-HA. Moreover, the highest value was observed in the 2% gastrodin-PU/n-HA group, which showed pronounced expression of ALP, RUNX2, and COL1 (Fig. 2D–F).

3.3. Macrophage behavior mediated by scaffolds

Macrophages were closely adhered and in numbers comparable to that on the gastrodin-PU/n-HA substrates. A progressive increase in cell number was observed in both the 1% and 2% gastrodin-PU/n-HA groups at day 3, with values significantly higher than that in the control; however, lower macrophage proliferative activity was observed in the 0.5% gastrodin-PU/n-HA group. Nonetheless, all substrates presented a microenvironment conducive to cell growth (Fig. 3A). mRNA expression of iNOS (M1) and mRNA expression of Arg-1 and CD206 (M2) in RAW 264.7 cells were further examined by RT-qPCR. As shown in Fig. 3B, compared to the other groups, the pro-inflammatory gene iNOS was significantly down-regulated in both the 1% and 2% gastrodin-PU/n-HA groups. In contrast, the expression levels of Arg-1 and CD206 were up-regulated in the gastrodin-PU/n-HA groups, especially 2% gastrodin-PU/n-HA. To further explore the effects of gastrodin-PU/n-HA on macrophage behavior, pro-inflammatory iNOS and pro-regenerative Arg-1 immunofluorescence staining analysis was performed (Fig. 3C–E). Results showed a notably higher optical density for Arg-1 and lower optical density for iNOS in the 2% gastrodin-PU/n-HA group compared with the other groups. Western blotting showed similar results, along with reduced TNF-α protein expression in gastrodin-PU/n-HA (Fig. 3F and G). Taken together, these findings suggest that PU/n-HA scaffolds with gastrodin incorporation can attenuate activated M1 polarization but induce M2 polarization.

3.4. Effects of scaffold/macrophage microenvironment on osteogenic differentiation of rBMSCs and angiogenesis of HUVECs

To assess the effects of macrophage immune response on osteogenic and angiogenic differentiation, we explored cell migration and related gene and protein expression levels in rBMSCs (Fig. 4A) and HUVECs (Fig. 5A) cultured in different conditioned media of scaffold-activated RAW 264.7 cells. The migratory abilities of rBMSCs treated with 1% and 2% gastrodin-PU/n-HA-activated RAW 264.7 cell media were enhanced compared with the other groups (Fig. 4B and C). Furthermore, the expression of osteogenic genes (BMP-2 and ALP) in rBMSCs was significantly enhanced in the gastrodin-PU/n-HA groups, especially the 2% gastrodin-PU/n-HA group (Fig. 4D and E). Correspondently, BMP-2 protein expression in the 2% gastrodin-PU/n-HA group was markedly increased, as shown by immunofluorescence staining (Fig. 4F and G) and western blotting (Fig. 4H and I). Similar to the rBMSCs, when treated with conditioned medium of 2% gastrodin-PU/n-HA-activated RAW 264.7 cells, the migratory ability of HUVECs was enhanced, and the expression of angiogenic markers (VEGF and BFGF) was significantly up-regulated at both the gene (Fig. 5D and E) and protein levels (Fig. 5F–J).

3.5. Altered initial immune/inflammatory responses to the scaffold in vivo

Immune/inflammatory response and angiogenesis elicited by the scaffolds by subcutaneous implantation were explored. As seen in Fig. 6B and C, IL-1β protein content in blood serum was significantly reduced in the 2% gastrodin-PU/n-HA group after 3 and 14 days. In

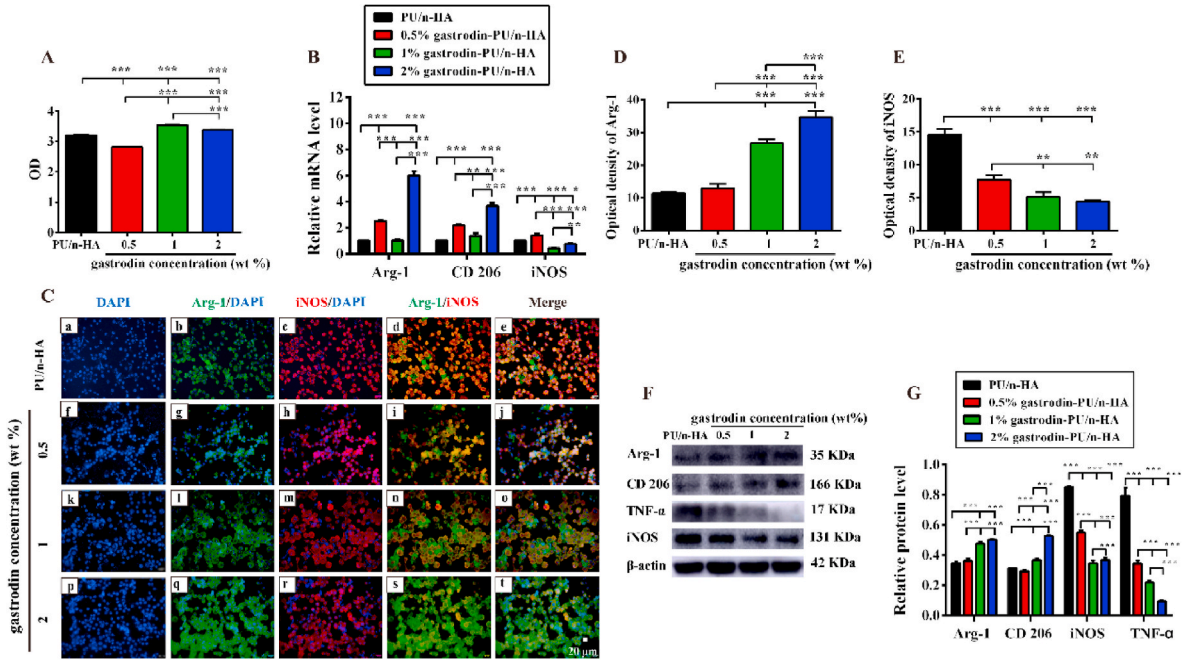

Fig. 3. Assessment of immunomodulatory effects of scaffolds on macrophages after 3 days of culture. (A) Viability of RAW 264.7 cells using CCK-8. (B) Relative gene expression levels of Arg-1, CD206, and iNOS. (C) Immunofluorescence staining of Arg-1 (green), iNOS (red), and nuclei (blue). (D, E) Quantitative analysis of optical density of (D) Arg-1 and (E) iNOS staining. (F) Arg-1, CD 206, iNOS, and TNF-α protein expression levels in RAW 264.7 cells measured by western blotting, and (G) calculated corresponding protein levels. Error bars represent standard deviation from mean (n = 3). ***$p < 0.001$; **$p < 0.01$; *$p < 0.05$. (For interpretation of the references to colour in this figure legend, the reader is referred to the Web version of this article.)

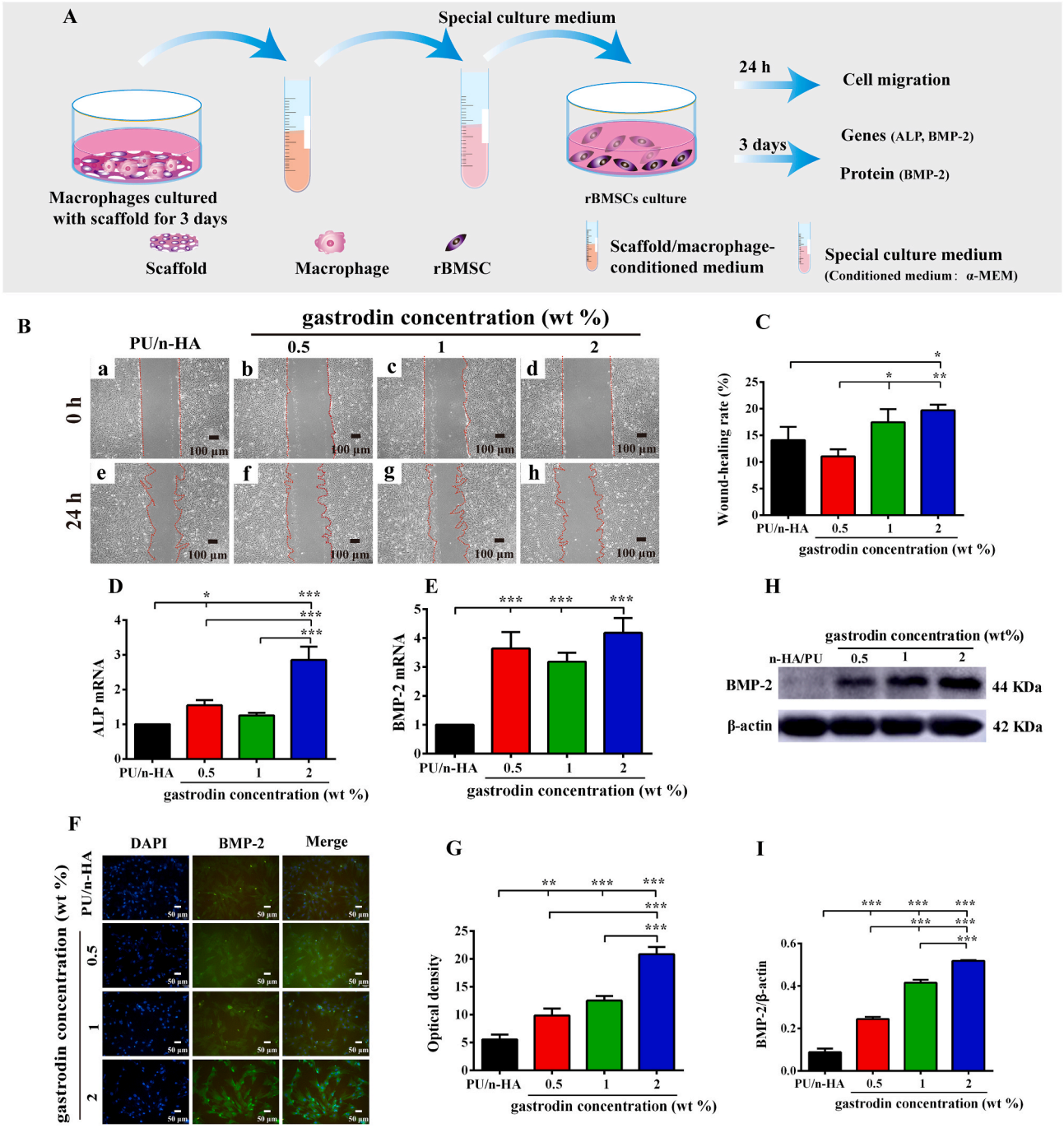

Fig. 4. (A) Schematic of osteogenic differentiation using conditioned medium from RAW 264.7 cells cultured with scaffolds for 3 days. (B) Cell migration in scratch assay. (C) Quantitative analysis of migratory ability of rBMSCs. (D, E) Osteogenic gene expression of ALP (D) and BMP-2 (E) analyzed by RT-qPCR. (F, G) Immunofluorescence staining of BMP-2 (F) and corresponding optical density (G). (H, I) Western blotting (H) and relative intensity of bands (I). Error bars represent standard deviation from mean (n = 3). $^{***}p < 0.001$; $^{**}p < 0.01$; $^{*}p < 0.05$.

contrast, the PU/n-HA group exhibited an inflammatory microenvironment with a significantly higher level of IL-1β protein. The Arg-1 macrophage population increased substantially in the 2% gastrodin-PU/n-HA group (Fig. 6D(d), E). Contrastly, the iNOS macrophage population decreased significantly compared with the PU/n-HA group on day 3 (Fig. 6D(a), F). On day 14, inflammatory cells remained robust in the PU/n-HA group (mainly iNOS cells) (Fig. 6D(e)), whereas very few were observed in the 2% gastrodin-PU/n-HA group (mainly Arg-1 cells) (Fig. 6D(h)). These results demonstrate that 2% gastrodin-PU/n-HA scaffolds can promote the polarization of macrophages to the M2 phenotype, thereby reducing the inflammatory response after implantation and allowing better integration with host tissue.

Histological observations showed that the inflammatory response around the subcutaneous gastrodin-PU/n-HA implants subsided after 14 days (Fig. 6G). In the PU/n-HA group, a thick fibrous capsule formed around the implant; however, the thickness of the fibrous capsule was markedly reduced in the gastrodin-PU/n-HA groups, especially the 2% gastrodin-PU/n-HA group. The thickness of the fibrous capsule in the PU/n-HA group was almost double that found in the gastrodin-PU/n-HA groups (Fig. 6H). The ability of the scaffolds to promote angiogenesis *in vivo* was further evaluated. A few small-caliber blood vessels appeared in the periphery of the 2% gastrodin-PU/n-HA scaffold (Fig. 6I(d, h)),

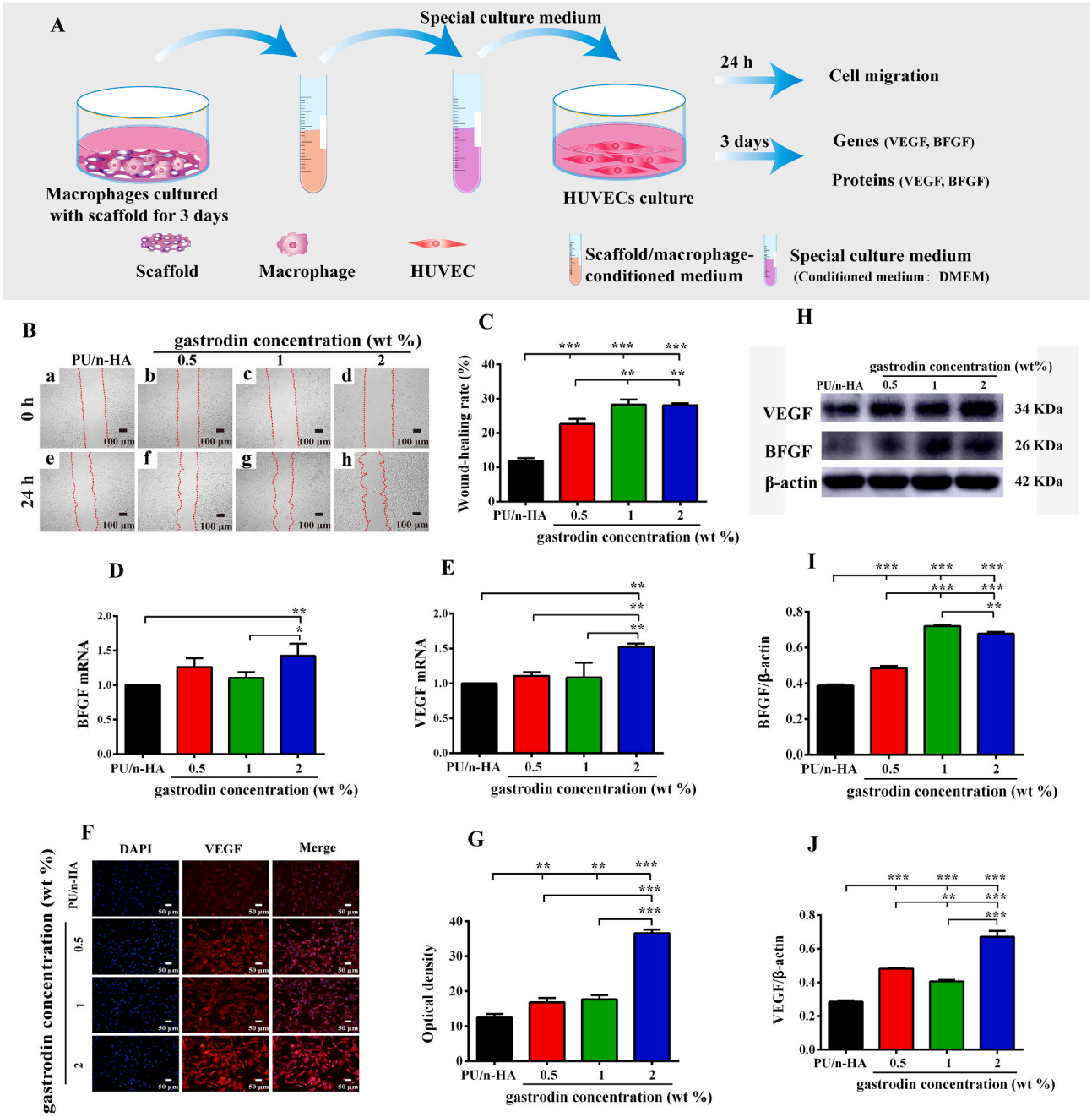

Fig. 5. (A) Schematic of angiogenic differentiation using conditioned medium from RAW 264.7 cells cultured with scaffolds for 3 days. (B) Cell migration in scratch assay. (C) Quantitative analysis of migratory ability of HUVECs. (D, E) Angiogenic gene expression of BFGF (D) and VEGF (E) analyzed by RT-qPCR. (F, G) Immunofluorescence staining of VEGF (F) and corresponding optical density (G). (H–J) Western blotting (H) and relative intensity of BFGF (I) and VEGF (J) bands. Error bars represent standard deviation from mean (n = 3). ***$p < 0.001$; **$p < 0.01$; *$p < 0.05$.

indicating its ability to effectively promote angiogenesis. The *ex vivo* co-culture experiments showed that the retrieved tissue samples from 2% gastrodin-PU/n-HA significantly enhanced tube formation in the HUVECs, as evidenced by increased branching and junction formation between cells (Fig. 6J and K). Additionally, no pathological changes in the heart, liver, spleen, lung, or kidney were found in histological specimens after 2 weeks (Fig. S8), indicating that the scaffolds did not cause local or systemic toxicity.

3.6. Regenerative potential of scaffold in bone defect model

New bone formation among the implants was evaluated at 4, 8, and 12 weeks postoperatively. Micro-CT imaging indicated that implantation of 2% gastrodin-PU/n-HA achieved the best bone defect healing outcome and showed apparent bridging of the defect. The newly formed bone tissue showed active and progressive reconstruction from weeks 4–12, as seen by the change in density at the defect region (Fig. 7A(c, f, i)). In contrast, PU/n-HA only achieved limited bridging with little penetration of bone tissue into the center of the porous scaffold (Fig. 7A(a, d, g)), while 1% gastrodin-PU/n-HA exhibited insufficient bridging, despite partial infiltration of bone tissue into the central area of the defect (Fig. 7A(b, e, h)). Quantitative micro-CT analysis demonstrated that the 2% gastrodin-PU/n-HA group achieved the highest total bone tissue formation (BV/TV) and trabecular thickness (Tb. Th), followed by 1% gastrodin-PU/n-HA and PU/n-HA (Fig. 7B and C). Of note, the regeneration of new bone tissue showed a time-

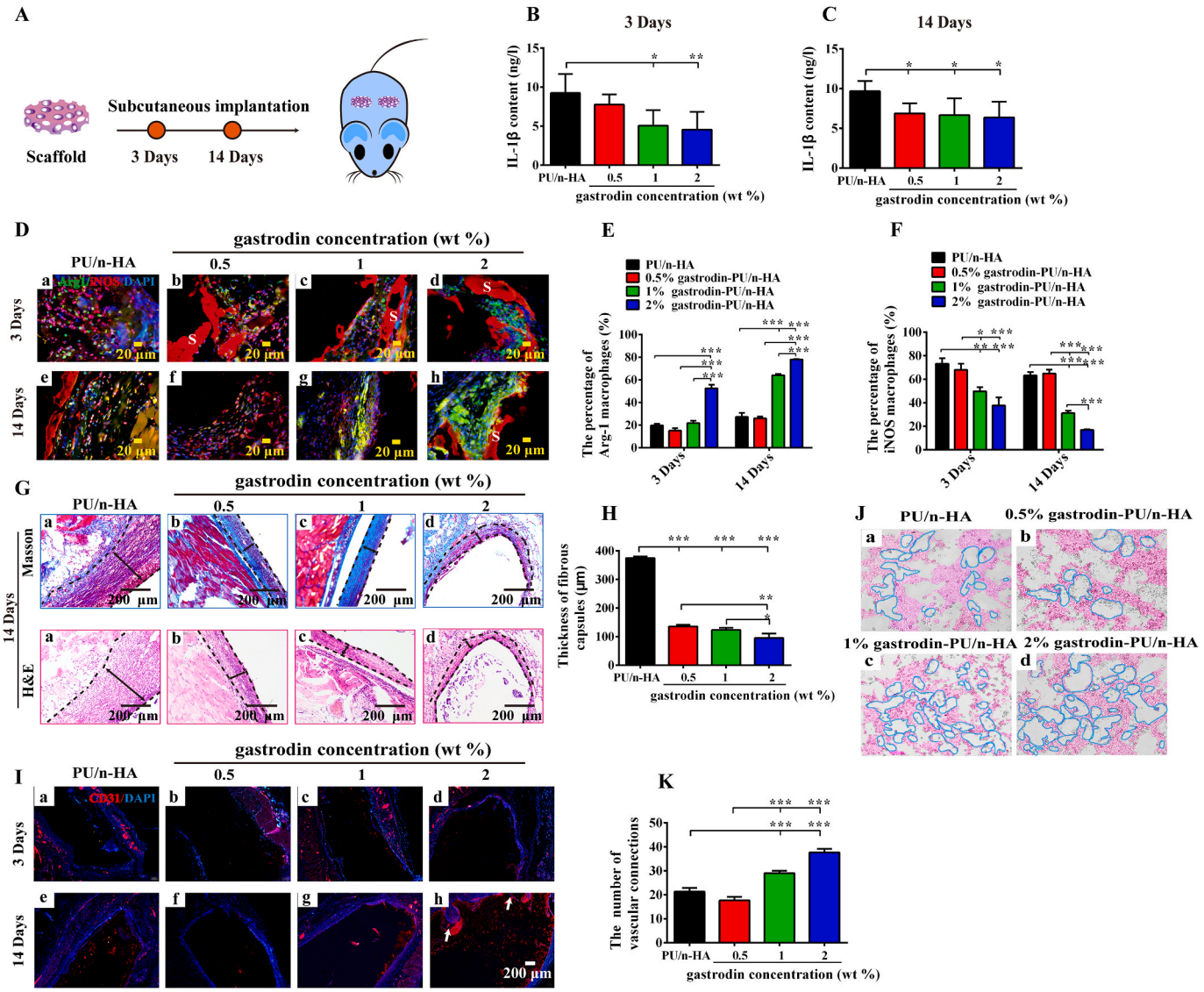

Fig. 6. Histological analysis of host response to gastrodin-PU/n-HA scaffolds following 2-week subcutaneous implantation. (A) Schema of subcutaneous implantation of scaffolds. (B, C) Content of IL-1β protein measured by ELISA assay at 3 (B) and 14 (C) days. (D) Immunofluorescence staining of PU/n-HA (a, e), 0.5% gastrodin-PU/n-HA (b, f), 1% gastrodin-PU/n-HA (c, g), and 2% gastrodin-PU/n-HA (d, h) at 3 (a–d) and 14 days (e–h). iNOS was used to label M1 macrophages with red signals, and Arg-1 was used to label M2 macrophages with green signals. (E, F) Quantitative analysis of (E) Arg-1 (M2) and (F) iNOS (M1) macrophage populations. (G) Masson and H&E staining of subcutaneous implanted scaffolds after 14 days. (H) Thickness of fibrous capsules surrounding implants. (I) CD31 staining. (J) Images and (K) quantitative analysis of vascular connections from *ex vivo* experiment to analyze gastrodin effects on HUVECs. S represents scaffolds; Two-way black arrows mark span of fibrous capsule at scaffold-tissue interface; White arrows indicate newly formed vessels. Error bars represent standard deviation from mean (n = 3). ***$p < 0.001$; **$p < 0.01$; *$p < 0.05$. (For interpretation of the references to colour in this figure legend, the reader is referred to the Web version of this article.)

dependent increase in all groups. The three-dimensional (3D) reconstructed images of the implants showed that the 2% gastrodin-PU/n-HA group had a looser structure and less volume with faster degradation of the scaffold from weeks 4–12 (Fig. 7D(c, f, i)), followed by the 1% gastrodin-PU/n-HA group. In contrast, PU/n-HA showed little degradation at 4 weeks, with partial degradation observed at weeks 8 and 12. Quantitative analysis also supported the superior performance of 2% gastrodin-PU/n-HA in promoting degradation (Fig. 7E), consistent with the *in vitro* results.

Histological analysis with Masson (Figs. 7F and S10) and H&E (Fig. S11) staining was performed to assess the bone tissue regeneration patterns within the porous scaffolds from weeks 4–12. Consistent with the micro-CT findings, the 2% gastrodin-PU/n-HA group showed accelerated defect healing, with continuous bone-like tissue bridging of the defects at all time points. At 4 weeks, several fibrous connective tissue formation islands (in blue) were observed within the pores of the 2% gastrodin-PU/n-HA scaffolds (Fig. 7F(c)), while sporadic fibrous connective tissue formation islands were observed in the pore structure and adjacent to the peripheral regions of the 1% gastrodin-PU/n-HA scaffolds (Fig. 7F(b)). In the PU/n-HA group (Fig. 7F(a)), almost no tissue formation was found within the porous scaffold. In the 2% gastrodin-PU/n-HA group, the bone formation islands grew rapidly and gradually replaced the fibrous tissue at 8 weeks (marked as NB, Fig. 7F (f)), and then further expanded and interconnected to form a large area of bone tissue (mature lamellar bone, yellow dotted line) at 12 weeks (Fig. 7F(i)). In addition, the 2% gastrodin-PU/n-HA implants integrated tightly with native bone tissue at the defect edges. The bone formation islands in the 1% gastrodin-PU/n-HA group proliferated more slowly and infiltrated the scaffold pores at 8 weeks, with bone formation (woven bone and cancellous bone-like tissue) in the central regions of the scaffold at 12 weeks (Fig. 7F(e, h)). In the PU/n-HA group, the osteoid tissues grew into the scaffold pores slowly from weeks 8 and 12

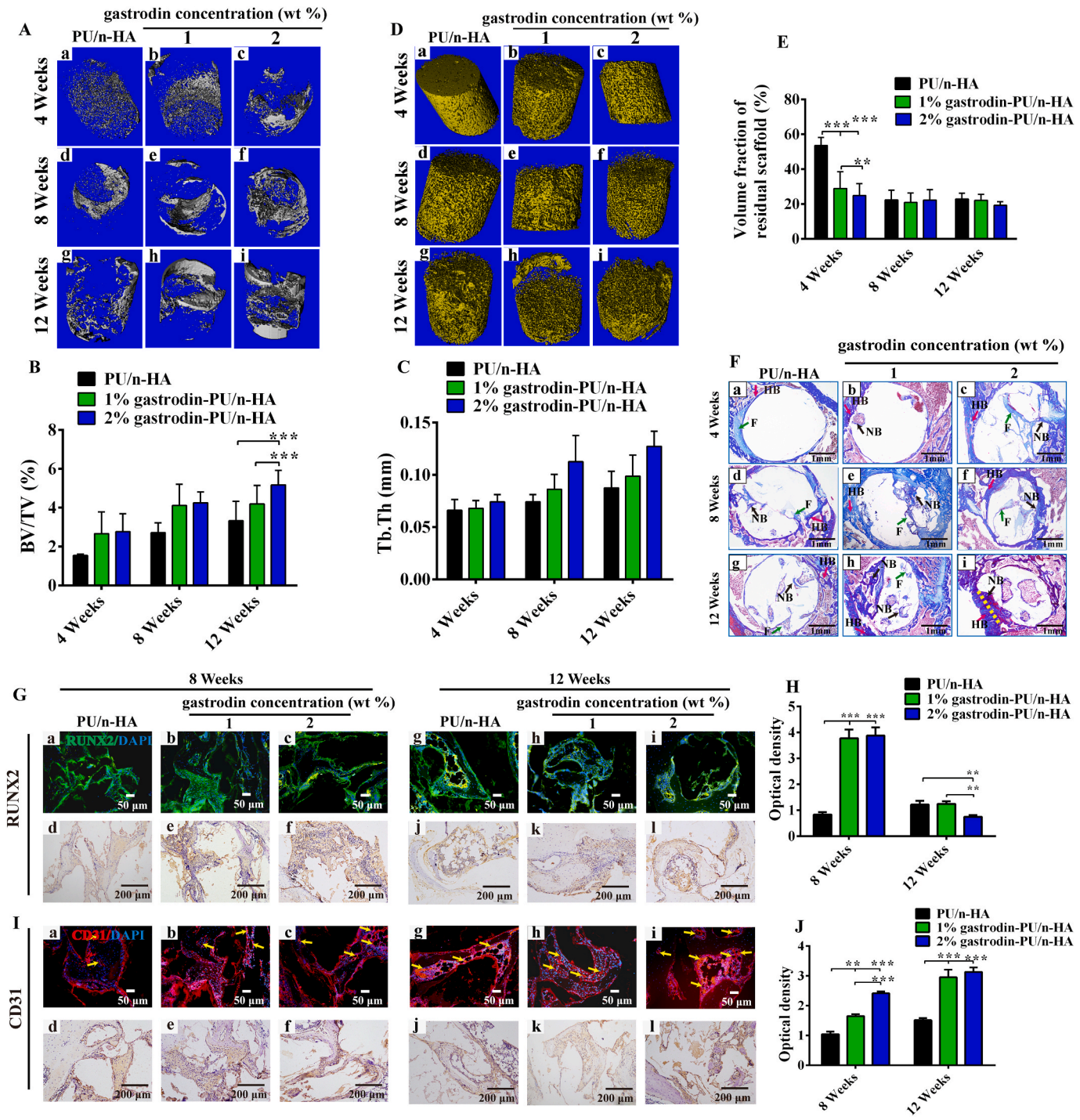

Fig. 7. *In vivo* bone regeneration at 4, 8, and 12 weeks after implantation of scaffolds in rat femoral condyle defects. (A) Micro-CT 3D images of new bones. (B) Bone volume/Total volume (BV/TV). (C) Trabecular thickness (Tb. Th). (D) 3D images and (E) Volume fraction of residual scaffold in defect areas. (F) Masson staining of PU/n-HA (a, d, g), 1% gastrodin-PU/n-HA (b, e, h), and 2% gastrodin-PU/n-HA (c, f, i). (G) Immunofluorescence and immunohistochemical staining of RUNX2 at 8 (a–f) and 12 weeks (g–l). (H) Quantitative analysis (immunohistochemical optical density within defect) of RUNX2 expression. (I) Immunofluorescence and immunohistochemical staining of CD31 at 8 (a–f) and 12 weeks (g–l). (J) Quantitative analysis (immunohistochemical optical density within defect) of CD31 expression. Green arrows mark "F- fibrous tissue"; Red arrows mark "HB-host bone"; Black arrows mark "NB-new bone"; Yellow dashed lines mark interface between HB and NB; Yellow arrows mark newly formed vessels. Error bars represent standard deviation from mean (n = 5). ***$p < 0.001$; **$p < 0.01$. (For interpretation of the references to colour in this figure legend, the reader is referred to the Web version of this article.)

(Fig. 7F(d, g)).

Immunofluorescence and immunohistochemical staining showed significantly higher RUNX2 expression localized in the new bone tissue of the gastrodin-PU/n-HA groups at 8 weeks than that in the PU/n-HA group (Fig. 7G(a - f)). With time, large amounts of mature bone tissue grew into the 2% gastrodin-PU/n-HA scaffold pores and were surrounded by reduced RUNX2 expression at 12 weeks (Fig. 7G(g - l), H). At this time point, both the 1% gastrodin-PU/n-HA and PU/n-HA groups showed higher RUNX2 staining intensity. RUNX2 plays an essential role in maintaining the supply of immature osteoblasts, leading to the

formation of immature bone that is easily resorbed; however, RUNX2 is suppressed for compact bone formation [57].

The growth and repair of the skeletal system involves CD31, which regulates angiogenesis. Here, expression of CD31 peaked at 8 weeks postoperatively (Fig. 7I(a - f)), followed by an increase at 12 weeks, with higher expression in the 2% gastrodin-PU/n-HA group than other groups throughout the whole study (Fig. 7I(g - l), J). In addition, due to the optimized loading of gastrodin, infiltration of blood vessels (yellow arrows) was evident within the new bone tissue, and staining of the vessels was intense over time in the 2% gastrodin-PU/n-HA group (Fig. 7I(c, i)). However, in the PU/n-HA group, while endothelial cells were positively stained, there were fewer blood vessels compared with that in the 2% and 1% gastrodin-PU/n-HA groups at later time points (Fig. 7I(g - i)). Blood vessel formation facilitates communication among pores, thus promoting angiogenesis and osteogenesis.

4. Discussion

Recent advances in tailoring biomaterials for directing macrophage fate for wound healing applications are encouraging. For regenerating bone defects, biomaterials with anti-inflammatory properties are needed to promote M2 macrophage polarization and create prohealing immune microenvironment [37]. Immunomodulatory biomaterials to efficiently synergize traditional therapies hold great promise to break through the bottleneck in regenerative process. Macrophages are an integral component of bone tissue, and their presence and immune response to biomaterials can create a wound healing microenvironment and modulate the recruitment of critical cells (such as MSCs) [58]. In addition to physical, chemical, and dynamic cues, a biomaterial designed to target macrophages that incorporates bioactive components capable of regulating the local microenvironment to direct the regeneration cascade is hailed as a potential strategy to enhance bone construction.

In the current study, we focused on design strategies of osteoimmunomodulatory biomaterials from the standpoint of integrated traditional Chinese herbal medicine and materials science to regulate macrophage fate. Research has shown that bioactive gastrodin exhibits certain pharmacological activities, including anti-necrotic, anti-apoptotic, anti-oxidative, and anti-inflammatory properties [59,60]. Our extended experiments revealed the therapeutic effects of gastrodin supplementation on osteodifferentiation in a dose-dependent manner. At a concentration of 10 μM, gastrodin significantly up-regulated the mRNA expression of RUNX2, ALP, and OCN in rBMSCs (Fig. S1), in agreement with previous study showing that gastrodin can alleviate glucocorticoid-induced osteoporosis in rats by protecting osteoblasts [43]. Huang et al. also showed that gastrodin can protect hBMSCs and RAW 264.7 cells from oxidative stress, ameliorate trabecular micro-architecture, and inhibit osteoclastogenesis in ovariectomized rats (OVX) [44]. However, as gastrodin is easily metabolized *in vivo*, we considered that gastrodin combined with PU could achieve sequential release of gastrodin, thereby reducing the inflammatory response (i.e., TNF-α and IL-1β levels) in RAW 264.7 cells [51]. Thus, we designed a gastrodin-delivery composite scaffold and explored its immunomodulatory effects on vascular bone regeneration.

In detail, gastrodin and n-HA were successfully incorporated into PU to construct a gastrodin-PU/n-HA composite scaffold (Figs. 1A and S2). The prepared composites had a compressive strength exceeding 3 MPa (Fig. 1E), although only 2% and 1% gastrodin-PU/n-HA had elastic moduli greater than 0.05 GPa (Fig. 1D). These results are equivalent to the mechanics of natural cancellous bone (mechanical strength >2 MPa, Young's modulus >0.05 GPa) [61], and thus should provide adequate supporting strength. The addition of gastrodin not only increased the crosslinking density of the composite scaffolds, thereby improving their mechanical properties [62], but also increased their hydrophilicity and promoted degradability [51], thus greatly improving functional regulation. Compared with the other gastrodin-PU/n-HA and PU/n-HA groups, the 2% gastrodin-PU/n-HA scaffold showed the highest mass loss in the PBS (Fig. S5A) and 0.5 M NaOH solutions (Fig. 1F). The higher indicator of molecular weight distribution (PDI, Table S4) in 2% gastrodin-PU/n-HA was vulnerable to attack, leading to the destruction and degradation of molecular structure. The *in vivo* biodegradability of the 2% gastrodin-PU/n-HA scaffold was also markedly enhanced (Fig. 7D(c, f, i)), which was beneficial for tissue growth into the defect (Fig. 7A(c, f, i)). Concomitantly, the enhanced release of gastrodin (Fig. 1G) was an important driver of immune microenvironment regulation conducive to angiogenesis and osteogenesis.

Accumulating evidence suggests that PU/n-HA hierarchical structured scaffolds can directly stimulate the osteogenic function of rBMSCs *in vitro* and enhance bone formation *in vivo* [55]. However, in a bone graft implantation situation, rBMSCs and immune cells are involved, and macrophages may be one of the first cell types recruited to the implant. Therefore, macrophage regulation towards balance is vital for understanding the interaction mechanisms of bone implants with the bone defect microenvironment [63]. In this study, we provided a new perspective that PU/n-HA decorated with anti-inflammatory gastrodin can enhance bone regeneration by manipulating the polarization of macrophages. Remarkably, the designed gastrodin-PU/n-HA scaffolds drove RAW 264.7 macrophages preferentially towards the M2 phenotype (Fig. 3B–G). Activated M2 macrophages participate in the clearance of debris, suppression of inflammation, and regulation of tissue regeneration [64]. Strikingly, compared to the other groups, the RAW 264.7 cells on the 2% gastrodin-PU/n-HA substrates reduced the expression of pro-inflammatory cytokines (i.e., iNOS and TNF-α) but elevated the production of anti-inflammatory cytokines (i.e., Arg-1 and CD206) (Fig. 3B–G). However, further studies are required to determine if the host response to biomaterials can also influence macrophage polarization. Following implantation with gastrodin-PU/n-HA scaffolds, higher numbers of Arg-1 (M2) macrophages were observed in the subcutaneous embedded model rats after 3 and 14 days, especially in the 2% gastrodin-PU/n-HA group (Fig. 6D(d, h), E). In contrast, M1 macrophages were dominant in the PU/n-HA group (Fig. 6D(a, e), F), indicative of a more pro-inflammatory microenvironment. Excessive or prolonged inflammatory events can lead to thick fibrous capsule formation and disturbed bone cell differentiation and blood vessel formation [65–67], thereby vastly delaying bone healing [68]. Our results showed that 14 days after subcutaneous implantation, fibrous capsule thickness in the gastrodin-PU/n-HA scaffold groups was less than half that in the PU/n-HA group (Fig. 6G and H). In addition to the inherent anti-inflammatory function of released gastrodin, an increase in the hydrophilicity of biomaterial is favorable for cell proliferation [69] and M2 polarization, and thus the anti-inflammatory effects of local microenvironments. On the other hand, higher hydrophobicity of biomaterial may induce macrophage polarization to the M1 phenotype by controlling fibrinogen adsorption and conformation [70]. Activated M2 macrophages in the 2% gastrodin-PU/n-HA group were therefore beneficial to the anti-inflammatory response as they possessed potential immunomodulatory and pro-regenerative properties.

Crosstalk between immune and bone-forming cells is essential to complete the inflammation stage and initiate new bone formation [25]. Therefore, we hypothesized that secretome from gastrodin-PU/n-HA-treated macrophages may enhance osteodifferentiation of rBMSCs in a gastrodin-loading-dependent manner to demonstrate the pro-osteogenic roles of these cytokines (i.e., Arg-1 and CD206). In brief, the rBMSCs were treated with gastrodin-PU/n-HA/macrophage-conditioned medium or PU/n-HA/macrophage-conditioned medium (Fig. 4A). Consistent with macrophage polarization, cell migration was accelerated (Fig. 4B and C) and the expression levels of osteogenic cytokines, such as BMP-2 and ALP, in the rBMSCs (Fig. 4D–I) were up-regulated in the gastrodin-PU/n-HA groups compared with the PU/n-HA group, with the 2% gastrodin-PU/n-HA-conditioned medium resulting in the highest expression. The direct contact experiments between rBMSCs and scaffolds also showed that the 2% gastrodin-PU/n-HA stimulated rBMSC osteodifferentiation (higher levels of RUNX2, ALP, COL1, Fig. 2D–F). These results could be

attributed to the regulation of the immune microenvironment via secretion of both anti-inflammatory and osteogenic cytokines.

Angiogenesis provides sufficient oxygen and nutrients to facilitate growth and differentiation and removes waste during the bone regeneration process [71]. As gastrodin-loaded PU can augment neo-vessel formation after subcutaneous implantation [51], we further investigated the angiogenic effects of macrophage polarization induced by gastrodin-PU/n-HA. The HUVECs were first treated with conditioned medium from different scaffold-activated macrophages (Fig. 5A). Results showed that the expression levels of angiogenic cytokines, such as VEGF and BFGF, were up-regulated by the gastrodin-PU/n-HA/macrophage-conditioned medium compared to the PU/n-HA/macrophage-conditioned medium, with the 2% gastrodin-PU/n-HA group showing the highest enhancement (Fig. 5D–J). When the HUVECs were cultured with tissue samples retrieved at day 3 (Fig. 6J and K), more extensive tubular networks were observed in the 2% gastrodin-PU/n-HA group compared with the other groups. The control showed no apparent vessels. The recruitment capability of macrophages strongly contributes to the repair process as they release cytokines and growth factors to enhance the function of tissue repair cells to regulate the damaged microenvironment [72]. In the current study, 2% gastrodin-PU/n-HA induced massive infiltration of M2 macrophages into the scaffold after implantation (Fig. 6D(d, h)). Macrophage accumulation due to proliferation was also evident *in vitro* in the 1% and 2% gastrodin-PU/n-HA groups at day 3. The macrophage population was significantly higher in these groups than in the PU/n-HA group (Fig. 3A). Moreover, bioactive molecules secreted by M2-polarized macrophages acted in synergy with the released gastrodin to promote the regulation of angiogenesis (VEGF and BFGF) (Fig. 5D–J). These results indicate that the 2% gastrodin-PU/n-HA-activated macrophages also affect angiogenesis. Biomaterial-regulated angiogenesis during tissue regeneration may act via multiple pathways, including direct stimulation of endothelial cells and indirect activation of macrophages.

Osteogenesis and angiogenesis are coordinated processes during lifelong bone formation. Increasing evidence supports the critical role of the immune microenvironment in these processes [73]. As mentioned above, the gastrodin-loaded PU/n-HA scaffolds may regulate the inflammatory response of macrophages and ultimately affect osteo/angio-differentiation. Thus, proper coordination plays a vital role in the entire bone repair process [74]. Here, the femoral defect model confirmed that 2% gastrodin-PU/n-HA treatment resulted in greater bone mass development than 1% gastrodin-PU/n-HA treatment or PU/n-HA treatment over a period of 12 weeks (Fig. 7A–C). In addition, 2% gastrodin-PU/n-HA demonstrated prominent osteointegration capability with the host bone, as shown by Masson staining (Fig. 7F). Thus, 2% gastrodin-PU/n-HA may be involved in regulating the local microenvironment at the early stages of the bone healing process, which could initiate rBMSC migration and osteodifferentiation to activate the systematic and well-orchestrated progression of downstream events. Furthermore, in the 2% gastrodin-PU/n-HA group, mature lamellar bone appeared at 12 weeks, RUNX2 expression in immature osteoblasts peaked at 8 weeks, and RUNX2 expression in mature osteoblasts decreased, indicating effective bone repair (Fig. 7G and H) [57]. Synchronously, many CD31-positive cells were detected in the 2% gastrodin-PU/n-HA group (Fig. 7I and J).

Our study showed that 2% gastrodin-PU/n-HA induced M2 polarization, regulated osteogenic differentiation, promoted HUVEC tube formation and angiogenesis, and contributed to bone regeneration in response to the local immune microenvironment (Fig. 8). We believe that the observed effect on macrophage polarization may be triggered and driven by the release of gastrodin, and that gastrodin-PU/n-HA mimicry is key to this effect. Thus, 2% gastrodin-PU/n-HA is a potential candidate for the development of immunomodulatory biomaterials. However, further studies are desirable to ascertain how the release of gastrodin modulates crucial chemokine/cytokine (i.e., SDF-1, IL-1β,

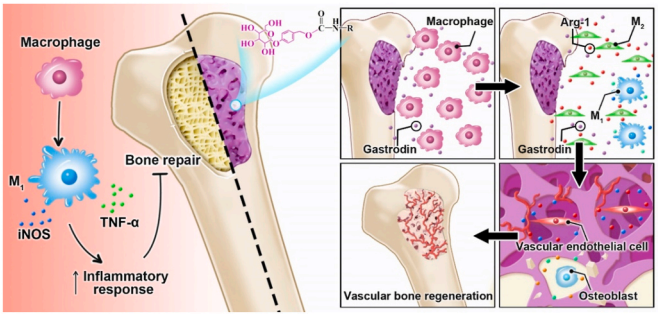

Fig. 8. Mechanism of macrophage-modulating gastrodin-PU/n-HA composite scaffold improved osteogenesis and angiogenesis.

Arg-1) secretion for recruited cells, notably macrophages. In addition, the underlying mechanism of immune microenvironment-induced bone regeneration needs to be clarified.

5. Conclusion

With the sustained release of gastrodin, gastrodin-PU/n-HA biomaterials exhibit good osteoimmunomodulatory properties, which are beneficial for the active osteodifferentiation of rBMSCs and angiogenesis of HUVECs. Specifically, 2% gastrodin-PU/n-HA induces M2 macrophage phenotype polarization and produces an optimal anti-inflammatory/immune microenvironment by controlling critical cell functions, such as migration, adhesion, and proliferation, consequently triggering maximized osteo-/angiogenic capacity. The functionalization of PU/n-HA with therapeutic gastrodin appears to modulate the inflammatory microenvironment to achieve superior bone regeneration outcomes, thus showing considerable potential in bone tissue engineering. Leveraging the roles of gastrodin and PU/n-HA will improve our understanding of biomaterial-macrophage interactions, and thus accelerate the development of new macrophage-based therapeutics in combination with integrated traditional Chinese medicine and biomaterial science.

CRediT authorship contribution statement

Limei Li: Investigation, Writing – original draft. **Qing Li:** Investigation, Data curation, Visualization. **Li Gui:** Resources, Formal analysis. **Yi Deng:** Formal analysis. **Lu Wang:** Investigation, Formal analysis. **Jianlin Jiao:** Investigation. **Yingrui Hu:** Investigation. **Xiaoqian Lan:** Investigation. **Jianhong Hou:** Supervision, Conceptualization. **Yao Li:** Resources, Conceptualization. **Di Lu:** Resources, Supervision, Conceptualization, Writing – review & editing.

Declaration of competing interest

The authors declare that they have no known competing financial interests or personal relationships that could have appeared to influence the work reported in this paper.

Acknowledgements

This research was supported by the National Natural Science Foundation of China (82160175/81860326), Department of Science and Technology of Yunnan Province of China (2017FF117(-062)/202101AY070001-078), and 100 Talents Program of Kunming Medical University (Limei Li).

Appendix A. Supplementary data

Supplementary data to this article can be found online at https://doi.org/10.1016/j.bioactmat.2022.03.037.

References

[1] V.V. Kozik, L.P. Borilo, E.S. Lyutova, A.S. Brichkov, Y.W. Chen, E.A. Izosimova, Preparation of CaO@TiO2–SiO2 biomaterial with a sol–gel method for bone implantation, ACS Omega 5 (42) (2020) 27221–27226, https://doi.org/10.1021/acsomega.0c03335.

[2] L.S. Zhu, D. Luo, Y. Liu, Effect of the nano/microscale structure of biomaterial scaffolds on bone regeneration, Int. J. Oral Sci. 12 (1) (2020) 6, https://doi.org/10.1038/s41368-020-0073-y.

[3] X.Q. Jiang, Biomaterials for bone defect repair and bone regeneration, Chin. J. Stomatol. 52 (2017) 600–604, https://doi.org/10.3760/cma.j.issn.1002-0098.2017.10.004.

[4] P.F. Gouveia, J. Mesquita-Guimarães, M.E. Galárraga-Vinueza, J.C.M. Souza, F. S. Silva, M.C. Fredel, A.R. Boccaccini, R. Detsch, B. Henriques, In-vitro mechanical and biological evaluation of novel zirconia reinforced bioglass scaffolds for bone repair, J. Mech. Behav. Biomed. Mater. 114 (2021), 104164, https://doi.org/10.1016/j.jmbbm.2020.104164.

[5] R. Dimitriou, E. Jones, D. McGonagle, P.V. Giannoudis, Bone regeneration: current concepts and future directions, BMC Med. 9 (1) (2011) 66, https://doi.org/10.1186/1741-7015-9-66.

[6] T. Einhorn, The cell and molecular biology of fracture healing, Clin. Orthop. Relat. Res. 355 (1998) S7–S21, https://doi.org/10.1097/00003086-199810001-00003.

[7] B. Yedekçi, A. Tezcaner, A.Z. Alshemary, B. Yılmaz, T. Demir, Z. Evis, Synthesis and sintering of B, Sr, Mg multi-doped hydroxyapatites: structural, mechanical and biological characterization, J. Mech. Behav. Biomed. Mater. 115 (2021), 104230, https://doi.org/10.1016/j.jmbbm.2020.104230.

[8] S.L. McNamara, E.M. McCarthy, D.F. Schmidt, S.P. Johnston, D.L. Kaplan, Rheological characterization, compression, and injection molding of hydroxyapatite-silk fibroin composites, Biomaterials 269 (2021), 120643, https://doi.org/10.1016/j.biomaterials.2020.120643.

[9] M.J. Dewey, A.V. Nosatov, K. Subedi, R. Shah, A. Jakus, B.A.C. Harley, Inclusion of a 3D-printed hyperelastic bone mesh improves mechanical and osteogenic performance of a mineralized collagen scaffold, Acta Biomater. 121 (2021) 224–236, https://doi.org/10.1016/j.actbio.2020.11.028.

[10] Y.F. Shao, X. Qing, Y. Peng, H. Wang, Z. Shao, K.Q. Zhang, Enhancement of mechanical and biological performance on hydroxyapatite/silk fibroin scaffolds facilitated by microwave-assisted mineralization strategy, Colloids Surf. B Biointerfaces 197 (2021) 111401, https://doi.org/10.1016/j.colsurfb.2020.111401.

[11] H.J. Haugen, S.P. Lyngstadaas, F. Rossi, G. Perale, Bone grafts: which is the ideal biomaterial? J. Clin. Periodontol. 46 (S21) (2019) 92–102, https://doi.org/10.1111/jcpe.13058.

[12] B. Safari, A. Aghanejad, L. Roshangar, S. Davaran, Osteogenic effects of the bioactive small molecules and minerals in the scaffold-based bone tissue engineering, Colloids Surf. B Biointerfaces 198 (2021), 111462, https://doi.org/10.1016/j.colsurfb.2020.111462.

[13] X.J. Wang, S.Q. Xu, S.W. Zhou, W. Xu, M. Leary, P. Choong, M. Qian, M. Brandt, Y. M. Xie, Topological design and additive manufacturing of porous metals for bone scaffolds and orthopaedic implants: a review, Biomaterials 83 (2016) 127–141, https://doi.org/10.1016/j.biomaterials.2016.01.012.

[14] S.A.O. Eming, T.A.O. Wynn, P.A.O. Martin, Inflammation and metabolism in tissue repair and regeneration, Science 356 (6342) (2017) 1026–1030, https://doi.org/10.1126/science.aam7928.

[15] J. He, G. Chen, M. Liu, Z. Xu, H. Chen, L. Yang, Y. Lv, Scaffold strategies for modulating immune microenvironment during bone regeneration, Mater. Sci. Eng. C Mater. Biol. Appl. 108 (2020) 110411, https://doi.org/10.1016/j.msec.2019.110411.

[16] Q.Y. Wang, Y.Q. Tang, Q.F. Ke, W.J. Yin, C.Q. Zhang, Y.P. Guo, J.J. Guan, Magnetic lanthanum-doped hydroxyapatite/chitosan scaffolds with endogenous stem cell-recruiting and immunomodulatory properties for bone regeneration, J. Mater. Chem. B 8 (24) (2020) 5280–5292, https://doi.org/10.1039/d0tb00342e.

[17] C.Z.W. Lee, T. Kozaki, F.A.O. Ginhoux, Studying tissue macrophages in vitro: are iPSC-derived cells the answer? Nat. Rev. Immunol. 18 (11) (2018) 716–725, https://doi.org/10.1038/s41577-018-0054-y.

[18] A. Alaarg, C. Pérez-Medina, J. Metselaar, M. Nahrendorf, Z. Fayad, G. Storm, W. Mulder, Applying nanomedicine in maladaptive inflammation and angiogenesis, Adv. Drug Deliv. Rev. 119 (2017) 143–158, https://doi.org/10.1016/j.addr.2017.05.009.

[19] R. Klopfleisch, Macrophage reaction against biomaterials in the mouse model-phenotypes, functions and markers, Acta Biomater. 43 (2016) 3–13, https://doi.org/10.1016/j.actbio.2016.07.003.

[20] M.K. Chang, L.J. Raggatt, K.A. Alexander, J.S. Kuliwaba, N.L. Fazzalari, K. Schroder, E.R. Maylin, V.M. Ripoll, D.A. Hume, A.R. Pettit, Osteal tissue macrophages are intercalated throughout human and mouse bone lining tissues and regulate osteoblast function in vitro and in vivo, J. Immunol. 181 (2) (2008) 1232, https://doi.org/10.4049/jimmunol.181.2.1232.

[21] S. Mukherjee, S. Darzi, A. Rosamilia, V. Kadam, Y. Truong, J.A. Werkmeister, C. E. Gargett, Blended nanostructured degradable mesh with endometrial mesenchymal stem cells promotes tissue integration and anti-inflammatory response in vivo for pelvic floor application, Biomacromolecules 20 (1) (2019) 454–468, https://doi.org/10.1021/acs.biomac.8b01661.

[22] K. Schmidt-Bleek, H. Schell, J. Lienau, N. Schulz, P. Hoff, M. Pfaff, G. Schmidt, C. Martin, C. Perka, F. Buttgereit, H.D. Volk, G. Duda, Initial immune reaction and angiogenesis in bone healing, J. Tissue Eng. Regen. Med. 8 (2) (2014) 120–130, https://doi.org/10.1002/term.1505.

[23] M. Novak, T. Koh, Macrophage phenotypes during tissue repair, J. Leukoc. Biol. 93 (2013), https://doi.org/10.1189/jlb.1012512.

[24] G. Juban, B. Chazaud, Metabolic regulation of macrophages during tissue repair: insights from skeletal muscle regeneration, FEBS Lett. 591 (2017) 3007–3021, https://doi.org/10.1002/1873-3468.12703.

[25] J.M. Sadowska, F. Wei, J. Guo, J. Guillem-Marti, Z.M. Lin, M.P. Ginebra, Y. Xiao, The effect of biomimetic calcium deficient hydroxyapatite and sintered β-tricalcium phosphate on osteoimmune reaction and osteogenesis, Acta Biomater. 96 (2019) 605–618, https://doi.org/10.1016/j.actbio.2019.06.057.

[26] R. Sridharan, A. Cameron, D. Kelly, C. Kearney, F. O'Brien, Biomaterial based modulation of macrophage polarization: a review and suggested design principles, Mater. Today 18 (6) (2015) 313–325, https://doi.org/10.1016/j.mattod.2015.01.019.

[27] D.W. Zhao, K.Q. Zuo, K. Wang, Z.Y. Sun, Y.P. Lu, L. Cheng, G.Y. Xiao, C. Liu, Interleukin-4 assisted calcium-strontium-zinc-phosphate coating induces controllable macrophage polarization and promotes osseointegration on titanium implant, Mater. Sci. Eng. C Mater. Biol. Appl. 118 (2021) 111512, https://doi.org/10.1016/j.msec.2020.111512.

[28] Z.J. Lin, D.N. Shen, W.X. Zhou, Y.F. Zheng, T.T. Kong, X.Y. Liu, S.L. Wu, P.K. Chu, Y. Zhao, J. Wu, K.M.C. Cheung, K.W.K. Yeung, Regulation of extracellular bioactive cations in bone tissue microenvironment induces favorable osteoimmune conditions to accelerate in situ bone regeneration, Bioact. Mater. 6 (8) (2021) 2315–2330, https://doi.org/10.1016/j.bioactmat.2021.01.018.

[29] M. Zou, J.C. Sun, Z. Xiang, Induction of M2-type macrophage differentiation for bone defect repair via an interpenetration network hydrogel with a GO-based controlled release system, Adv. Healthc. Mater. 10 (2021), e2001502, https://doi.org/10.1002/adhm.202001502.

[30] B. Brown, B. Ratner, S. Goodman, S. Amar, S. Badylak, Macrophage polarization: an opportunity for improved outcomes in and regenerative medicine, Biomaterials 33 (2012) 3792–3802, https://doi.org/10.1016/j.biomaterials.2012.02.034.

[31] H.Z. Shen, J. Shi, Y. Zhi, X.Y. Yang, Y. Yuan, J. Si, S.G.F. Shen, Improved BMP2-CPC-stimulated osteogenesis in vitro and in vivo via modulation of macrophage polarization, Mater. Sci. Eng. C Mater. Biol. Appl. 118 (2021), 111471, https://doi.org/10.1016/j.msec.2020.111471.

[32] C.E. Witherel, P.L. Kubinski, K.L. Spiller, In vitro model of macrophage-biomaterial interactions, Methods Mol. Biol. 1758 (2018) 161–176, https://doi.org/10.1007/978-1-4939-7741-3_13.

[33] B.H. Cha, S.R. Shin, J. Leijten, Y.C. Li, S. Singh, J.C. Liu, N. Annabi, R. Abdi, M. R. Dokmeci, N.E. Vrana, A.M. Ghaemmaghami, A. Khademhosseini, Integrin-mediated interactions control macrophage polarization in 3D hydrogels, Adv. Healthc. Mater. 6 (21) (2017), 1700289, https://doi.org/10.1002/adhm.201700289.

[34] G.M. Sun, Pro-regenerative hydrogel restores scarless skin during cutaneous wound healing, Adv. Healthc. Mater. 6 (23) (2017), 1700659, https://doi.org/10.1002/adhm.201700659.

[35] Z. Chen, A. Bachhuka, S. Han, F. Wei, S. Lu, R.M. Visalakshan, K. Vasilev, Y. Xiao, Tuning chemistry and topography of nanoengineered surfaces to manipulate immune response for bone regeneration applications, ACS Nano 11 (5) (2017) 4494–4506, https://doi.org/10.1021/acsnano.6b07808.

[36] J.A. Jones, D.T. Chang, H. Meyerson, E. Colton, I.K. Kwon, T. Matsuda, J. M. Anderson, Proteomic analysis and quantification of cytokines and chemokines from biomaterial surface-adherent macrophages and foreign body giant cells, J. Biomed. Mater. Res. 83 (3) (2007) 585–596, https://doi.org/10.1002/jbm.a.31221.

[37] F. Lebre, C. Hearnden, E. Lavelle, Modulation of immune responses by particulate materials, Adv. Mater. 28 (27) (2016) 5525–5541, https://doi.org/10.1002/adma.201505395.

[38] Y.L. Xie, W.C. Sun, F.F. Yan, H.W. Liu, Z.M. Deng, L. Cai, Icariin-loaded porous scaffolds for bone regeneration through the regulation of the coupling process of osteogenesis and osteoclastic activity, Int. J. Nanomed. 14 (2019) 6019–6033, https://doi.org/10.2147/IJN.S203859.

[39] S.F. Chen, H. Liang, Y.H. Ji, H.W. Kou, C. Zhang, G.W. Shang, C.F. Shang, Z. M. Song, L. Yang, L. Liu, Y.K. Wang, H.J. Liu, Curcumin modulates the crosstalk between macrophages and bone mesenchymal stem cells to ameliorate osteogenesis, Front. Cell Dev. Biol. 9 (2021), 634650, https://doi.org/10.3389/fcell.2021.634650.

[40] Z.W. Peng, S.Q. Wang, G.J. Chen, M. cai, R. Liu, J. Deng, J.Z. Liu, T. Zhang, Q. R. Tan, C.X. Hai, Gastrodin alleviates cerebral ischemic damage in mice by improving anti-oxidant and anti-inflammation activities and inhibiting apoptosis pathway, Neurochem. Res. 40 (4) (2015) 661–673, https://doi.org/10.1007/s11064-015-1513-5.

[41] H.N. Wang, R.G. Zhang, Y.T. Qiao, F. Xue, H. Nie, Z.J. Zhang, Y. Wang, Z.W. Peng, Q.R. Tan, Gastrodin ameliorates depression-like behaviors and up-regulates proliferation of hippocampal-derived neural stem cells in rats: involvement of its anti-inflammatory action, Behav. Brain Res. 266 (2014) 153–160, https://doi.org/10.1016/j.bbr.2014.02.046.

[42] J.N. Dai, Y. Zong, L.M. Zhong, Y.M. Li, W. Zhang, L.G. Bian, Q.L. Ai, Y.D. Liu, L. Juan, D. Lu, Gastrodin inhibits expression of inducible NO synthase, cyclooxygenase-2 and proinflammatory cytokines in cultured LPS-stimulated

microglia via MAPK pathways, PLoS One 6 (2011), e21891, https://doi.org/10.1371/journal.pone.0021891.
[43] S.Y. Liu, L. Zhou, L.Y. Yang, S. Mu, T. Fang, Q. Fu, Gastrodin alleviates glucocorticoid induced osteoporosis in rats via activating the Nrf2 signaling pathways, Oncotarget 9 (14) (2018) 11528–11540, https://doi.org/10.18632/oncotarget.23936.
[44] Q. Huang, J. Shi, B. Gao, H.Y. Zhang, J. Fan, X.J. Li, J.Z. Fan, Y.H. Han, J.K. Zhang, L. Yang, Z.J. Lu, J. Liu, Gastrodin: an ancient Chinese herbal medicine as a source for anti-osteoporosis agents via reducing reactive oxygen species, Bone 73 (2015) 132–144, https://doi.org/10.1016/j.bone.2014.12.059.
[45] L. Hu, Y. Sun, Y. Wu, Advances in chitosan-based drug delivery vehicles, Nanoscale 5 (8) (2013) 3103–3111, https://doi.org/10.1039/c3nr00338h.
[46] T. Ahmed, B. Aljaeid, Preparation, characterization, and potential application of chitosan, chitosan derivatives, and chitosan metal nanoparticles in pharmaceutical drug delivery, Drug Des. Dev. Ther. 10 (2016) 483, https://doi.org/10.2147/DDDT.S99651.
[47] S. Wendels, L. Avérous, Biobased polyurethanes for biomedical applications, Bioact. Mater. 6 (4) (2021) 1083–1106, https://doi.org/10.1016/j.bioactmat.2020.10.002.
[48] A. Shababdoust, M. Zandi, M. Ehsani, P. Shokrollahi, R. Foudazi, Controlled curcumin release from nanofibers based on amphiphilic-block segmented polyurethanes, Int. J. Pharm. 575 (2020), 118947, https://doi.org/10.1016/j.ijpharm.2019.118947.
[49] H. Tian, Z. Tang, X. Zhuang, X. Chen, X. Jing, Biodegradable synthetic polymers: preparation, functionalization and biomedical application, Prog. Polym. Sci. 37 (2) (2012) 237–280, https://doi.org/10.1016/j.progpolymsci.2011.06.004.
[50] R. LogithKumar, A. KeshavNarayan, S. Dhivya, A. Chawla, S. Saravanan, N. Selvamurugan, A review of chitosan and its derivatives in bone tissue engineering, Carbohydr. Polym. 151 (2016) 172–188, https://doi.org/10.1016/j.carbpol.2016.05.049.
[51] M. Zheng, J.Z. Guo, Q. Li, J. Yang, Y. Han, H.C. Yang, M.L. Yu, L.M. Zhong, D. Lu, L.M. Li, L. Sun, Syntheses and characterization of anti-thrombotic and anti-oxidative Gastrodin-modified polyurethane for vascular tissue engineering, Bioact. Mater. 6 (2) (2021) 404–419, https://doi.org/10.1016/j.bioactmat.2020.08.008.
[52] Q. Li, L.M. Li, M.L. Yu, M. Zheng, Y. Li, J. Yang, M. Dai, L.M. Zhong, L. Sun, D. Lu, Elastomeric polyurethane porous film functionalized with gastrodin for peripheral nerve regeneration, J. Biomed. Mater. Res. 108 (8) (2020) 1713–1725, https://doi.org/10.1002/jbm.a.36937.
[53] L.M. Li, M.H. Zhao, J.D. Li, Y. Zuo, Q. Zou, Y.B. Li, Preparation and cell infiltration of lotus-type porous nano-hydroxyapatite/polyurethane scaffold for bone tissue regeneration, Mater. Lett. 149 (2015) 25–28, https://doi.org/10.1016/j.matlet.2015.02.106.
[54] L.M. Li, J.D. Li, Q. Zou, Y. Zuo, B. Cai, Y.B. Li, Enhanced bone tissue regeneration of a biomimetic cellular scaffold with co-cultured MSCs-derived osteogenic and angiogenic cells, Cell Prolif. 52 (2019), e12658, https://doi.org/10.1111/cpr.12658.
[55] L.M. Li, Y. Zuo, Q. Zou, B.Y. Yang, L.L. Lin, J.D. Li, Y.B. Li, Hierarchical structure and mechanical improvement of an n-HA/GCO-PU composite scaffold for bone regeneration, ACS Appl. Mater. Interfaces 7 (40) (2015) 22618–22629, https://doi.org/10.1021/acsami.5b07327.
[56] H.H. Liu, L. Zhang, J.D. Li, Q. Zou, Y. Zuo, W.D. Tian, Y.B. Li, Physicochemical and biological properties of nano-hydroxyapatite-reinforced aliphatic polyurethanes membranes, J. Biomater. Sci. Polym. Ed. 21 (2010) 1619–1636, https://doi.org/10.1163/092050609X12524778957011.
[57] Z. Maruyama, C. Yoshida, T. Furuichi, N. Amizuka, M. Ito, R. Fukuyama, T. Miyazaki, H. Kitaura, K. Nakamura, T. Fujita, N. Kanatani, T. Moriishi, K. Yamana, W. Liu, H. Kawaguchi, K. Nakamura, T. Komori, Runx2 determines bone maturity and turnover rate in postnatal bone development and is involved in bone loss in estrogen deficiency, Dev. Dynam. 236 (2007) 1876–1890, https://doi.org/10.1002/dvdy.21187.
[58] J.H. Li, X.Q. Jiang, H.J. Li, M. Gelinsky, Z. Gu, Tailoring materials for modulation of macrophage fate, Adv. Mater. 33 (2021), e2004172, https://doi.org/10.1002/adma.202004172.
[59] H.F. Zheng, E.P. Yang, H. Peng, J.P. Li, S. Chen, J.L. Zhou, H.S. Fang, B. Qiu, Z. Wang, Gastrodin prevents steroid-induced osteonecrosis of the femoral head in rats by anti-apoptosis, Chin. Med. J. (Engl). 127 (22) (2014) 3926–3931, https://doi.org/10.3760/cma.j.issn.0366-6999.20141371.
[60] C.L. Hsieh, J.J. L, S.Y. Chiang, S.Y. Su, N.Y. Tang, G.G. Lin, I.H. Lin, C.H. Liu, C. Y. Hsiang, J.C. Chen, T.Y. Ho, Gastrodia elata modulated activator protein 1 via c-Jun N-terminal kinase signaling pathway in kainic acid-induced epilepsy in rats, J. Ethnopharmacol. 109 (2) (2007) 241–247, https://doi.org/10.1016/j.jep.2006.07.024.
[61] G. Cama, L.L. Hench, G. Cama, Woodhead publishing. an introduction to bioceramic, 2013, in: L.L. Hench (Ed.), Chapter: Technology Transfer to Bioceramics: from Concept to Commerce, Imperial College Press, 2013.
[62] L.M. Li, Q. Li, J. Yang, L. Sun, J.Z. Guo, Y.Y. Yao, L.M. Zhong, D. Lu, Enhancement in mechanical properties and cell activity of polyurethane scaffold derived from gastrodin, Mater. Lett. 228 (2018) 435–438, https://doi.org/10.1016/j.matlet.2018.06.061.
[63] X.F. Ji, X. Yuan, L.M. Ma, B. Bi, H. Zhu, Z.H. Lei, W.B. Liu, H.X. Pu, J.W. Jiang, X. L. Jiang, Y. Zhang, J. Xiao, Mesenchymal stem cell-loaded thermosensitive hydroxypropyl chitin hydrogel combined with a three-dimensional-printed poly (ε-caprolactone)/nano-hydroxyapatite scaffold to repair bone defects via osteogenesis, angiogenesis and immunomodulation, Theranostics 10 (2) (2020) 725–740, https://doi.org/10.7150/thno.39167.
[64] A. Mantovani, S.K. Biswas, M.R. Galdiero, A. Sica, M. Locati, Macrophage plasticity and polarization in tissue repair and remodelling, J. Pathol. 229 (2) (2013) 176–185, https://doi.org/10.1002/jcp.26429.
[65] T.A. Wynn, T.R. Ramalingam, Mechanisms of fibrosis: therapeutic translation for fibrotic disease, Nat. Med. 18 (7) (2012) 1028–1040, https://doi.org/10.1038/nm.2807.
[66] J.E. Won, Y. Lee, J.H. Park, J.H. Lee, Y. Shin, C. Kim, J. Knowels, H.W. Kim, Hierarchical microchanneled scaffolds modulate multiple tissue-regenerative processes of immune-responses, angiogenesis, and stem cell homing, Biomaterials 227 (2019), 119548, https://doi.org/10.1016/j.biomaterials.2019.119548.
[67] F. O'Brien, Biomaterials & scaffolds for tissue engineering, Mater. Today 14 (2011) 88–95, https://doi.org/10.1016/S1369-7021(11)70058-X.
[68] H. Schell, G. Duda, A. Peters, S. Tsitsilonis, K. Johnson, K. Schmidt-Bleek, The haematoma and its role in bone healing, J. Exp. Orthop. 4 (1) (2017) 5, https://doi.org/10.1186/s40634-017-0079-3.
[69] Y. Yang, T. Zhang, M.Y. Jiang, X.J. Yin, X.Y. Luo, H.Q. Sun, Effect of the immune responses induced by implants in a integrated three-dimensional micro-nano topography on osseointegration, J. Biomed. Mater. Res. 30 (2020), e37134, https://doi.org/10.1002/jbm.a.37134.
[70] L. Lv, Y.T. Xie, K. Li, T. Hu, X. Lu, Y.Z. Cao, X.B. Zheng, Unveiling the mechanism of surface hydrophilicity-modulated macrophage polarization, Adv. Healthc. Mater. 7 (19) (2018), e1800675, https://doi.org/10.1002/adhm.201800675.
[71] M.C. Shi, L.G. Xia, Z.T. Chen, F. Lv, H.Y. Zhu, F. Wei, S.W. Han, J. Chang, Y. Xiao, C.T. Wu, Europium-doped mesoporous silica nanosphere as an immune-modulating osteogenesis/angiogenesis agent, Biomaterials 144 (2017) 176–187, https://doi.org/10.1016/j.biomaterials.2017.08.027.
[72] L. Boscá, M. Zeini, P.G. Traves, S. Hortelano, Nitric oxide and cell viability in inflammatory cells: a role for NO in macrophage function and fate, Toxicology 208 (2005) 249–258, https://doi.org/10.1016/j.tox.2004.11.035.
[73] P.C. Qiu, M.B. Li, K. Chen, B. Fang, P.F. Chen, Z.B. Tang, X.F. Lin, S.W. Fan, Periosteal matrix-derived hydrogel promotes bone repair through an early immune regulation coupled with enhanced angio- and osteogenesis, Biomaterials 227 (2019), 119552, https://doi.org/10.1016/j.biomaterials.2019.119552.
[74] P. Mountziaris, A. Mikos, Modulation of the inflammatory response for enhanced bone tissue regeneration, Tissue Eng. B Rev. 14 (2) (2008) 179–186, https://doi.org/10.1089/ten.teb.2008.0038.